Nano Research

Open Access

Review Article

Atomic-precision oxygen evolution materials: From empirical trial-and-error to AI-driven intelligent manufacturing

Yang Xiao[1,2,§], Bo Wang[1,2,§], Weizuo Li[3,§], Jianuo Liu[1,2], Xinru Ren[4], Cheng Qian[1,2], Xiugeng Ye[1,2], Jiangcheng Shi[1,2], Huang Zhou[1,2], Yafei Zhao[1,2] ✉, and Yuen Wu[1,2] ✉

[1] *State Key Laboratory of Precision and Intelligent Chemistry, School of Chemistry and Materials Science, University of Science and Technology of China, Hefei 230026, China*
[2] *Deep Space Exploration Laboratory, University of Science and Technology of China, Hefei 230026, China*
[3] *Key Laboratory of Advanced Catalytic Materials and Technology, Advanced Catalysis and Green Manufacturing Collaborative Innovation Center, Changzhou University, Jiangsu Province, Changzhou 213164, China*
[4] *School of Chemistry and Chemical Engineering, University of Jinan, Jinan 250022, China*
§ *Yang Xiao, Bo Wang, and Weizuo Li contributed equally to this work.*

Cite this article: *Nano Research*, **2026**, *19*, 94908378. https://doi.org/10.26599/NR.2026.94908378

ABSTRACT: As a key bottleneck in proton exchange membrane water electrolysis (PEMWE) for hydrogen production, the acidic oxygen evolution reaction (AOER) poses significant challenges due to its harsh reaction environment and sluggish kinetics. Addressing this bottleneck relies heavily on advancing atomic-precision oxygen evolution materials (APOEM). Traditional empirical trial-and-error (ETAE) approaches, while laying foundational groundwork, are inefficient in navigating the vast compositional and structural space of APOEM. They often fail to precisely tailor active sites to achieve balanced activity, stability, and cost, which limits progress in overcoming the intrinsic limitations. APOEM, by contrast, enables atomic-level control over active site configuration, ligand environments, and electron structures. This precision is critical for optimizing the adsorption/desorption kinetics of reaction intermediates and mitigating catalyst dissolution under acidic conditions, thus addressing the shortcomings of ETAE-driven material development. This review systematically summarizes the synergistic effects of atomic-level engineering, mechanistic insights, and artificial intelligence (AI)-driven screening in enhancing APOEM performance. Subsequently, four atomic-scale engineering strategies, including single-atom/clusters, defects, interfaces, and strain, are systematically reviewed. Finally, this review explores how AI-driven intelligent manufacturing (ADIM) transforms APOEM development. ADIM integrates AI, machine learning, high-throughput computing, and automated synthesis. Unlike ETAE, which relies on manual experimentation and serendipity, ADIM accelerates the screening of APOEM candidates, predicts structure–property relationships, and optimizes atomic configurations at scale.

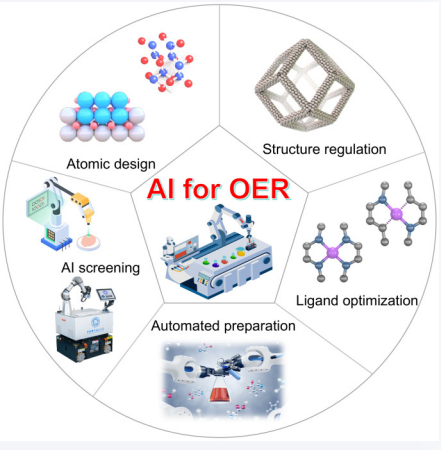

KEYWORDS: material manufacturing, oxygen evolution reaction, mechanisms, trial-and-error, artificial intelligence

1 Introduction

Green hydrogen produced via proton-exchange-membrane water electrolyzers (PEMWEs) is widely recognized as the linchpin of a carbon-neutral energy economy. PEMWEs enable hydrogen production with a purity exceeding 99.999 vol.%, achieve high current densities at relatively low cell voltages, and exhibit excellent responsiveness to intermittent renewable energy inputs [1–7]. These advantages are critical for advancing sustainable energy systems, but their full potential hinges on addressing challenges in the acidic oxygen evolution reaction (AOER) [8–10]. As a four-electron, four-proton process responsible for O_2 generation, AOER remains a persistent bottleneck that heavily influences the overall efficiency of system, durability, and cost, making the development of high-performance atomic-precision oxygen evolution materials (APOEM) essential to overcome it.

Compared with the relatively straightforward two-electron hydrogen evolution reaction, the AOER demands additional

Received: November 20, 2025; **Revised:** December 26, 2025
Accepted: December 26, 2025

✉Address correspondence to Yafei Zhao, yafeizhao@ustc.edu.cn; Yuen Wu, yuenwu@ustc.edu.cn

overpotential, triggers severe oxidative degradation of catalysts, and relies predominantly on rare and costly iridium or ruthenium oxides [11–15]. It also faces considerable challenges: high operational potentials cause APOEM dissolution and structural reconfiguration, while its multi-step reaction mechanism (involving *OH, *O, and *OOH intermediates) introduces intrinsic energy barriers [16–19]. Currently, only expensive and scarce Ir- and Ru-based oxides can deliver sufficient activity and stability for AOER, and traditional empirical trial-and-error (ETAE) approaches struggle to navigate the vast compositional and structural space of AOER materials [20–23]. This inefficiency often leads to "blind design" that fails to balance activity, stability, and cost. So, underscoring the need for APOEM and innovative development paradigms like AI-driven intelligent manufacturing (ADIM), is desired.

Single-atom catalysts (SACs) have attracted significant attention due to their unique ability to maximize the utilization efficiency of precious metals by dispersing isolated metal atoms across a support matrix [24–28]. Yet the isolated nature of their active sites creates substantial hurdles for facilitating the multi-electron and proton transfer processes inherent to AOER, resulting in sluggish reaction kinetics and reduced stability under acidic conditions. To tackle this intrinsic kinetic limitation, atomic-level engineering, a core strategy for fabricating APOEM, has emerged as a powerful approach. It enhances catalytic performance through precise modulation of active sites via atomic design, structural regulation, and ligand optimization [29, 30]. In addition, traditional ETAE approaches could modulate multiple adjacent metal centers arranged as dimers, trimers, or larger clusters in some cases, thereby promoting *O–*O bond formation and supports spatial control over reaction pathways [31–33]. With the advancement of chip technology and optimization of computing power, ADIM–integrating artificial intelligence (AI), machine learning (ML), high-throughput computing, and automated synthesis, has greatly accelerated the screening and prediction of optimal APOEM configurations across broad compositional spaces. When integrated with automated synthesis robots, these advanced systems enable researchers to systematically analyze large-scale datasets and identify complex structure–property relationships that are difficult or impossible to discern using conventional ETAE or analytical approaches [34–36].

Despite the abundance of reviews discussing acidic OER mechanisms or individual material systems, there is a distinct lack of comprehensive summaries that bridge the gap between atomic-precision engineering and the emerging paradigm of ADIM [37, 38]. Most existing literature treats material synthesis and AI screening as separate topics. Uniquely, this review integrates these domains, proposing a holistic roadmap that evolves from traditional ETAE to a closed-loop system combining AI and robotic synthesis. We argue that the extreme structural sensitivity of APOEMs (e.g., precise interatomic spacing for OPM pathways) specifically necessitates this transition to ADIM, offering a new perspective on how to overcome the efficiency bottlenecks in discovering next-generation PEMWE catalysts.

This review (Fig. 1) focuses on APOEM, exploring mechanistic insights into electrocatalytic active site behavior, strategic design principles for Ir-, Ru-, Co-, and Mn-based APOEM, and ADIM-driven high-throughput screening methodologies. In doing so, it aims to advance the development of next-generation APOEM and accelerate the industrial deployment of PEMWEs for sustainable hydrogen production.

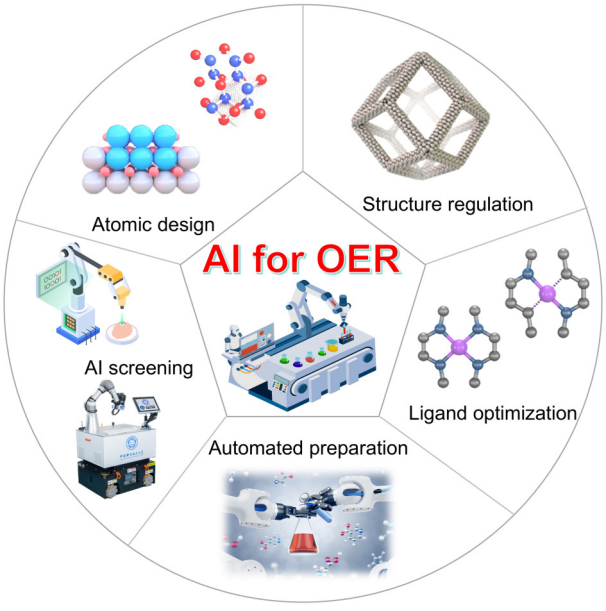

Figure 1 The overview of recent advanced strategies from ETAE to ADIM. This schematic illustrates the paradigm shift from traditional trial-and-error methods to AI-driven intelligent manufacturing, integrating atomic design, mechanism insights, and robotic automation.

2 Reaction mechanisms and advanced design strategies for APOEM

Inspired by the coordination environment of metal centers in conventional metal oxides, including both the first-shell M–O bonds and the second-shell M–O–M linkages (where M represents a metal), the AOER can exhibit a diverse range of complex yet highly tunable mechanistic pathways. The AOER involves intricate multi-electron and proton-coupled electron transfer processes, where multiple reaction pathways can lead to the formation of diverse intermediates and distinct energy profiles. Consequently, the AOER mechanism not only determines the intrinsic catalytic activity but also significantly affects APOEM stability under harsh operational conditions. A thorough understanding of these reaction pathways is essential for the rational design and optimization of APOEM. Recent advancements in spectroscopic characterization and theoretical simulation techniques have facilitated the investigation of dynamic structural transformations in APOEM and the identification of oxygen-containing reaction intermediates generated during the AOER. Among the most widely recognized reaction mechanisms are the adsorbate evolution mechanism (AEM), the lattice oxygen mechanism (LOM), and the oxide path mechanism [39–41]. This review presents a systematic analysis of these mechanisms and summarizes the key factors recently identified to influence AOER pathways. These insights provide a foundational basis for the development of more effective strategies in the design and optimization of APOEM.

3 Reaction mechanisms of AOER

Adsorbate evolution mechanism (AEM): The AEM pathway is preferred when the O 2p band center is at a low level, rendering lattice oxygen inert. This mechanism maintains structural integrity in harsh acidic electrolytes; however, it is restricted by the scaling relationships of intermediate binding energies. The conventional AEM primarily centers on water oxidation occurring at single-

metal sites, encompassing processes such as water dissociation and proton-coupled electron transfer (PCET). The typical elementary steps involve the formation and transformation of surface-bound hydroxyl (*OH), oxo (*O), and hydroperoxo (*OOH) intermediates, through successive PCET steps occurring on isolated metal active sites [42–44]. The process can be described in terms of the following elementary reaction steps

$$M + H_2O \rightarrow M-OH + H^+ + e^- \quad (1)$$

$$M-OH \rightarrow M-O + H^+ + e^- \quad (2)$$

$$M-O + H_2O \rightarrow M-OOH + H^+ + e^- \quad (3)$$

$$M-OOH \rightarrow M + O_2 + H^+ + e^- \quad (4)$$

A universal challenge in the AEM is the linear scaling relationship, which assumes a constant difference between the binding energies of M–OH and M–OOH species (ΔG^*_{OOH} = ΔG^*_{OH} + 3.2 eV) across various metal and metal oxide surfaces. According to the scaling relationship, when $\Delta G^*_O - \Delta G^*_{OH}$ and $\Delta G^*_{OOH} - \Delta G^*_O$ reach their optimal values, the theoretical minimum overpotential of 0.37 V can be achieved, thereby establishing a universal volcano-type correlation between catalytic activity and the adsorption energies of key intermediates.

Although the aforementioned scaling relationship constraints limit the maximum achievable activity, AEM involves only surface-adsorbed intermediates and does not perturb the bulk lattice structure, thereby avoiding oxygen vacancy formation or lattice reconstruction, which is particularly favorable under the harsh corrosive environment of AOER. Although scaling relationship constraints limit the maximum achievable activity, the AEM involves only surface-adsorbed intermediates and preserves the bulk lattice structure, thereby avoiding oxygen vacancy formation or structural reconstruction. This feature makes AEM particularly advantageous under the harsh corrosive conditions of AOER. Consequently, significant research efforts have been devoted to overcoming the theoretical scaling relationship in order to enhance intrinsic catalytic activity, through strategies such as strain engineering, vacancy creation, elemental doping, and interfacial engineering between the APOEM and the electrolyte.

Lattice oxygen mechanism (LOM): In acidic media, the initiation of LOM is highly reliant on the metal-oxygen covalency. As suggested by the rigid band model, a more substantial overlap between the metal-d and oxygen-p orbitals promotes the injection of holes into lattice oxygen, thereby activating the LOM pathway. Nevertheless, this occurs at the expense of thermodynamic stability owing to the formation of oxygen vacancies. Some APOEM have been reported to surpass the limitations imposed by the volcano relationship. To account for this discrepancy, the LOM has been proposed, which incorporates a critical step involving direct O–O coupling through the direct participation of lattice oxygen atoms in the catalytic cycle [43–46]. The entire reaction process can be summarized as follows

$$O_L-M + H_2O \rightarrow O_L-M-OH + H^+ + e^- \quad (5)$$

$$O_L-M-OH \rightarrow O_L-M-O + H^+ + e^- \quad (6)$$

$$O_L-M-O \rightarrow V_O-M^* + O_2 \quad (7)$$

$$V_O-M^* + H_2O \rightarrow M-OH + H^+ + e^- \quad (8)$$

$$M-OH \rightarrow O_L-M + H^+ + e^- \quad (9)$$

where O_L and V_O represent the involved lattice oxygen and surface oxygen vacancy, respectively. Due to the energy gap associated with the oxidation of lattice oxygen, the LOM can overcome the scaling relationships inherent in the AEM, thereby often resulting in enhanced oxygen evolution activity. Unlike the four PCET steps in AEM, LOM follows a distinct five-step reaction sequence. In contrast to the four PCET steps involved in AEM, LOM proceeds through a unique five-step reaction pathway. The process begins with the formation of adsorbed *O intermediates, which is achieved through two consecutive deprotonation steps (Eqs. (5) and (6)). These intermediates subsequently undergo coupling with lattice oxygen atoms, resulting in the evolution of O2 and the simultaneous formation of surface oxygen vacancies (Eq. (7)). The involvement of lattice oxygen is a key characteristic that distinguishes the LOM mechanism from the conventional AEM. The catalytic cycle proceeds as water molecules replenish the oxygen vacancies (Eq. (8)), thereby regenerating the active sites and maintaining the ongoing reaction (Eq. (9)). The LOM pathway circumvents the scaling relationship constraints by bypassing *OOH formation, although this advantage is often accompanied by a reduction in structural stability.

Oxide path mechanism (OPM): The prerequisite for OPM under acidic conditions is strictly geometric. In contrast to AEM, which occurs at single sites, OPM necessitates adjacent metal sites with an optimal distance (typically approximately 3 Å) to promote the direct coupling of oxo–intermediates. This geometric descriptor is crucial for the design of stable Ru/Ir arrays that prevent lattice consumption. Compared with AEM and LOM, OPM offers distinct advantages for developing efficient APOEM, as it enables the direct coupling of two *O species on adjacent metal sites, without the need for oxygen vacancies or the formation of additional *OOH intermediates. By facilitating the direct coupling of two *O species on adjacent metal sites, OPM operates without requiring oxygen vacancies or the generation of *OOH intermediates [47–49]. In contrast to the AEM and LOM pathways, which rely on isolated M–O octahedra, an alternative O–O direct coupling mechanism can occur at adjacent multinuclear sites, typically facilitated by M–O–M bridging motifs. By eliminating the dependence on oxygen vacancies or the involvement of additional *OOH intermediates, the OPM mechanism offers a theoretical approach to overcoming activity limitations while maintaining APOEM stability. Central to the OPM mechanism is a process in which two neighboring metal centers undergo deprotonation of *OH groups at precisely controlled distances, leading to the formation of two M–O species (Eqs. (12) and (13)). These mechanisms can be systematically summarized as follows

$$M-M + H_2O \rightarrow M-M-OH + H^+ + e^- \quad (10)$$

$$M-M-OH + H_2O \rightarrow HO-M-M-O + 2H^+ + 2e^- \quad (11)$$

$$HO-M-M-O \rightarrow O-M-M-O + H^+ + e^- \quad (12)$$

$$O-M-M-O \rightarrow M-M+O_2 \quad (13)$$

Considerable efforts have been devoted to the development of APOEM that can effectively facilitate the OPM pathway. To enable efficient O–O coupling, APOEM must not only exhibit appropriate metal site spacing and geometric configurations, but also facilitate the stable adsorption of *O species and maintain suitable reaction energy barriers. Wang et al. systematically examined several potential O–O coupling pathways involving Co_{IV}(O) and Co_{IV}(OH) groups, cluding nucleophilic attack by solvent water molecules on terminal oxygen species, as well as lattice oxygen O–O coupling in cobalt oxide APOEM. Nevertheless, all of these pathways were found to be energetically unfavorable. The critical O–O bond formation step was determined to proceed via the direct coupling of two Co_{IV}(O) metaloxy groups [50].

To facilitate efficient O–O bond formation, APOEM must possess appropriately spaced metal sites with optimal geometric configurations, enabling the effective stabilization of *O intermediates and precise modulation of reaction energy barriers. Operating without lattice-oxygen migration or the replenishment of surface oxygen vacancies, this pathway inherently safeguards the integrity of the APOEM framework. Furthermore, the real-time identification of key reaction intermediates requires precise atomic-level control over APOEM structures, highlighting the central role of advanced *in-situ* characterization techniques in elucidating reaction mechanisms. The investigation into the mechanism of the OER is far from over. With the continuous advancement of *in-situ* characterization techniques, the intricate details of the OER are gradually being revealed.

4 Empirical trial-and-error strategy for APOEM

The configuration of active sites typically influences the binding energy, spatial arrangement, and density of oxygen intermediates, which in turn shapes the corresponding OER pathways. Meanwhile, variations in reaction mechanisms exert a substantial impact on the catalytic activity and stability of AOER systems. It is noteworthy that theoretical mechanisms need to be verified through experimental observations. Recent progress in *in-situ* and *operando* characterization techniques has been of great significance in this respect. For instance, to differentiate between the AEM and OPM pathways, Chang et al. employed electrochemical attenuated total reflectance surface-enhanced IR spectroscopy to monitor the dynamic evolution of surface species on Ru atom arrays [51]. They effectively observed the key intermediates related to direct O–O coupling, offering strong evidence for the OPM mechanism. Furthermore, the structural stability of APOEMs often exhibits dynamic characteristics. Lin et al. utilized advanced characterization techniques to disclose the *in-situ* reconstruction of Ru atom arrays on α-MnO_2, verifying that the active phase is formed under operating conditions [52]. These findings emphasize that APOEMs are not static entities; instead, they undergo complex evolution that determines their catalytic fate.

These considerations have spurred recent research efforts to systematically identify the critical factors that govern reaction mechanisms. Thus, APOEM and the design of active site ensembles stand as key elements to prioritize in the rational development of efficient APOEM, where precise control over active site features is far more impactful than the random adjustments inherent to ETAE approaches. The following are the key directions that the traditional ETAE approaches have taken into consideration.

Active sites distance: The OPM pathway, which enables direct O–O coupling between adjacent adsorbed *O species, not only breaks the activity limitations imposed by the AEM but also avoids the poor stability associated with oxygen vacancy formation in the LOM mechanism. This reaction pathway has been validated in homogeneous iron complexes and subsequently in OER materials under alkaline conditions [51]. However, despite recent advancements such as the introduction of cationic defects to enhance the synergistic interaction of dual-metal active sites, realizing OPM under acidic conditions continues to be a significant challenge. Recently, Lee and co-workers designed and synthesized an arrayed configuration of Ru atoms on α-MnO_2, wherein the adjacent Ru sites enabled the successful realization of the OPM pathway (Figs. 2(a) and 2(b)) [52]. The prevailing view holds that the core of the OPM mechanism lies in the presence of adjacent active sites. Therefore, regulating the distance between active sites to promote direct O–O coupling is considered a key strategy for increasing the contribution of the OPM pathway. Thereby, both the activity and durability of AOER are significantly enhanced.

Metal-oxygen covalency: Recent studies have indicated that the chemical characteristics of the M–O bond in iridium oxides or ruthenium oxides serve as a key descriptor for both O_2 desorption and H_2O adsorption on metal oxides [53]. The energy gap between the O 2p band and the M d band can serve as an indicator of metal-oxygen covalency, showing a strong correlation with the reactivity of lattice oxygen. The metal-oxygen bonds with weakened covalency make the redox of lattice oxygen more energetically unfavorable [54]. While stronger metal-oxygen covalency could facilitate metal atoms to accept more electrons from the energetically proximate O 2p orbitals during the redox processes [55, 56]. By collecting different OER performances of various oxides, an empirical linear regression model was proposed to correlate stretched Ir–O bonds and OER overpotential in these amorphous iridium oxides (Fig. 2(c)). A more flexible range of Ir–O bond lengths could increase the ability to tailor a more electrophilic O species to boost the OER performance [57]. Based on this theory, Wang and co-workers designed a layer $LiCoO_2$ support which is capable of dynamically regulating Ru–O covalency through the extraction and insertion of Li^+. The two-dimensional diffusion and extraction of Li^+ within the interlayer of the $LiCoO_2$ achieve the dynamic self-optimization of the RuO_2/$LiCoO_2$ interface, which moderately weakens the covalency of the Ru–O bond, suppressing the participation of lattice oxygen and achieving a good balance between catalytic activity and stability [58].

Recently, Lee and co-worker have systematically studied the electronic structure and electrochemical stability of different metastable nanoporous and amorphous IrO_2. As shown in Fig. 2(d), in crystalline IrO_2, the volumetric changes to the intercalated nanoporous IrO_2 defer to the channel size and intercalation ions, which further influence the bond length of Ir–O. The changed Ir–O length has an important impact on the bonding strength and covalency of the Ir–O bond, which will be important in creating different configurations of active sites and the determination of reaction mechanisms [59].

O 2p band center: The electronic structure is frequently emphasized, as it directly relates to the reactivity of metal sites and lattice oxygen in nanocrystalline APOEM. Importantly, the O 2p band center has been regarded as an appropriate descriptor for evaluating the oxygen vacancy formation energy and surface oxygen exchange kinetics in solid APOEM. Adjusting the energy

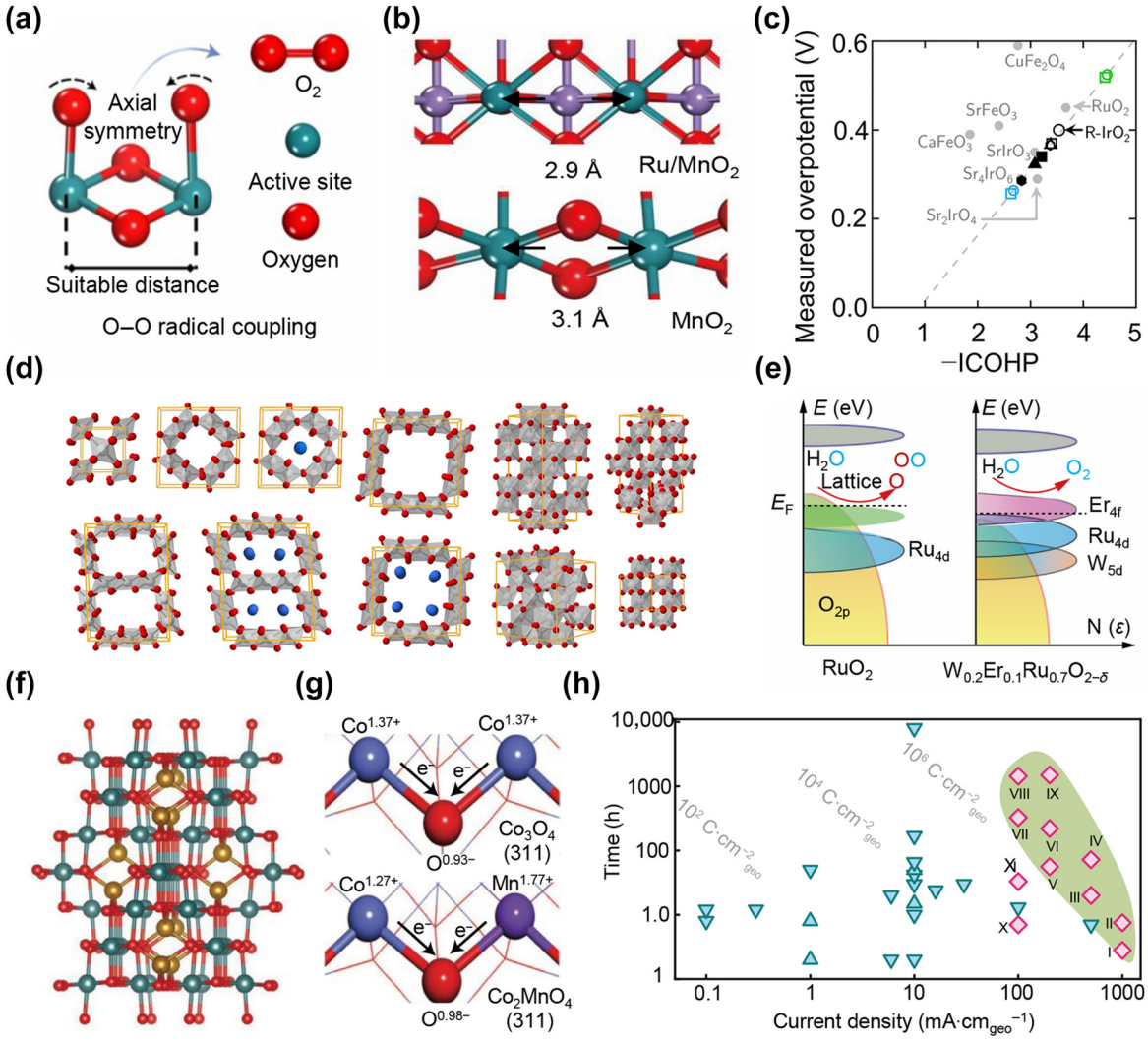

Figure 2 (a) O–O radical coupling promoted by symmetric dual active sites and (b) Ru–Ru interatomic distances in RuO_2 and α-MnO_2 with Ru atoms substituting for the Mn at surface sites. Reproduced with permission from Ref. [52], © Lin, C. et al. 2021. (c) Empirical regression model for structure–property relations in various APOEM. Reproduced with permission from Ref. [59], © Lee, S. et al. 2022. (d) Atomic and crystal structures of the crystalline iridium oxides. Reproduced with permission from Ref. [59], © Lee, S. et al. 2022. (e) Schematic diagrams of rigid band models for RuO_2 and $W_{0.2}Er_{0.1}Ru_{0.7}O_{2-\delta-1}$ toward AOER. Reproduced with permission from Ref. [60], © Hao, S. Y. et al. 2020. (f) Crystal structure of Co_2MnO_4, (g) the oxidation state of Co_3O_4 and Co_2MnO_4 described by differences in electron transfer based on Bader charge calculations, and (h) a comparison of the stability of Co_2MnO_4 with Co_3O_4 and other Earth-abundant APOEM. Reproduced with permission from Ref. [62], © Li, A. et al. 2022.

gap between the O 2p band center and the Fermi level can enhance the reactivity of lattice oxygen, thereby facilitating electron loss during electrochemical oxidation processes. thereby partially activating the reactivity of lattice oxygen and increasing the contribution of the LOM pathway during OER. It is widely accepted that the O 2p band center is a key factor governing the transition between AEM and LOM, influencing OER activity in perovskite oxides, spinel oxides, and transition metal (oxy)hydroxides under alkaline conditions. Recently, the O 2p band center theory has also been applied to explain and guide the design of highly durable RuO_2 for AOER. For example, Zhang and co-workers doped W and Er into the RuO_2 lattice, which widened the energy gap between the O 2p band center and the Fermi level (Fig. 2(e)), increased the oxygen vacancy formation energy, and significantly enhanced the long-term stability of RuO_2 [60]. Similarly, Wei and co-workers suppressed the LOM pathway by downshifting the O 2p band center [61], effectively locking the lattice oxygen and greatly reducing its participation in the AOER process.

Arrangement spacing of metal atoms: To overcome the activity limitations associated with a single active site, the construction of multiple catalytic sites that exhibit synergistic effects is essential for directing reaction pathways, thereby enhancing both the reaction rate and selectivity. For APOEM, when the spacing between metal atoms approaches a characteristic reaction threshold, the interactions among these atoms become notably significant. Such synergistic effects not only modulate the binding modes of adsorbed intermediates and establish sequentially linked active sites, but also facilitate the formation of novel reaction pathways, thereby collectively enhancing the reaction kinetics. Co-based materials have also emerged as promising non-noble metal candidates for AOER catalysis. For example, Co_3O_4 is known to be more active than MnO_2 under acid conditions. Stabilizing the structure of Co_3O_4 remains a major challenge for the development of Co-based

APOEM. Recently, Co_2MnO_4, which exhibits an activation energy for AOER comparable to that of state-of-the-art IrO_2, has been developed by incorporating Mn into the Co_3O_4 spinel lattice (Fig. 2(f)). Even if several Co atoms are leaching from the Co_2MnO_4, the Mn–rich surfaces still exhibit optimal binding energies. Encouragingly, benefiting from a stronger Mn–O bond and the high thermodynamic stability of lattice oxygen (Fig. 2(g)), Co_2MnO_4 catalysts can work over 2 months at 200 mA·cm^{-2} at pH = 1 without decreasing activity (Fig. 2(h)) [62].

To be specific, elongated metal spacing is unfavorable for the *O coupling, directing the reaction pathway towards AEM which occurs on a single site. However, excessively short metal distances may lead to shortened bond lengths between the metal and lattice oxygen, triggering their orbital hybridization and switching the reaction mechanism to the LOM. Recent works have demonstrated that two adjacent metal centers with a suitable distance undergo the formation of *O. These *O species can then directly couple, subsequently release an O_2 molecule. Except for the distance between metal atoms, the spatial arrangement and connectivity of M–O octahedra critically influence the OER pathway by modulating interatomic distances, geometric distortions, and electronic structures. In contrast, corner-sharing geometries with moderate metal spacing strike a balance between orbital hybridization and structural stability, bypassing serious structural deformation caused by excessive oxygen vacancies in LOM.

Although the empirical trial-and-error strategies have offered fundamental understandings of OER mechanisms and identified key descriptors (e.g., metal-oxygen covalency and O 2p band center), they are becoming increasingly inadequate to fulfill the stringent requirements of practical PEMWEs. The intrinsic randomness and low efficiency of these traditional methods often find it difficult to fundamentally solve the long-standing trade-off between activity and stability in harsh acidic environments. Consequently, to tackle the critical issues of noble metal scarcity and high costs, there is an urgent necessity to transition from macroscopic empirical adjustment to precise atomic-level engineering. This paradigm shift lays the groundwork for the rational design strategies of APOEM discussed in the subsequent section, which aim to optimize atom utilization and intrinsic durability.

5 Recent advances in APOEM trial-and-error strategy for APOEM

The development of efficient and durable APOEM is a cornerstone of increasing the overall energy efficiency of PEMWEs. The demand for industrialization drives the minimization of noble metal usage in PEMWEs, especially those of iridium and ruthenium, stand out as APOEM due to their high activity and stability. Nonetheless, Ir and Ru are expensive, averaging at US$162,279 kg^{-1} of Ir and US$16,090 kg^{-1} of Ru. The scarcity and price of Ir and Ru have spurred efforts to reduce their usage when considering costs and the scale-up of PEM electrolysis. Beyond a fundamental understanding of the OER mechanism and influencing factors, the practical design strategies for different types of APOEM, primarily Ir-based, Ru-based, and non-precious metal APOEM such as Mn-based and Co-based systems, have also become a central focus. reducing Ir loading while enhancing its intrinsic activity, in order to lower the manufacturing cost of PEMWEs and improve overall energy efficiency, ultimately facilitating the industrial implementation of PEMWEs.

Current research focuses on improving their durability to make them low-cost APOEM as potential substitutes for Ir-based materials. Meanwhile, the development of Mn- and Co-based APOEM involves stabilizing their metastable active phases and enhancing their acid resistance. Therefore, downsizing noble metals to fabricate the APOEM is an attractive strategy to maximize the metal atom utilization and minimize the costs without compromising the catalytic activity [63]. To optimize the effectiveness of each metal atom, every atomic site needs to contribute to an accelerated reaction and retain this performance over extended use. These requirements are challenging for AOER, where catalytic performance must be balanced against extreme corrosion and dissolution conditions. More importantly, atomically dispersed or ensemble metal active centers reduce the complexity of the catalytic pathways, enabling the use of simple and well-defined atomic-scale models to understand the OER mechanism. Herein, we provide an overview of recent research progress on Ir-based, Ru-based, Mn-based, and Co-based APOEM and summarize representative strategies for catalyst design. These tailored design approaches, guided by mechanistic insights, are paving the way toward next-generation catalysts of OER for practical application in acidic environments.

Single atoms to atomic arrays of APOEM: Recently, SACs with unique electronic structure, maximized atom utilization efficiency, and unsaturated coordination environment have sparked huge interest. Introducing Ru/Ir single atoms is effective as this strategy can effectively tune the coordination environments of surface Ru/Ir and subsurface oxygen, modulate the dynamic changes in Ru/Ir oxidation states during AOER, accelerate PCET steps, and optimize the adsorption energies of key OER intermediates. Atomically dispersed Ir-based APOEM typically incorporate Ir species at the atomic level into the lattice of supporting materials, often metal oxides. The unique coordination environments at these isolated Ir sites confer distinctive AOER activity and significantly improve Ir utilization. In supports that are intrinsically inert toward AOER, the density of atomic Ir sites plays a major role in determining the apparent catalytic activity. Nakamura and co-workers reported that atomically dispersed high-valent Ir in MnO_2 delivered an impressive mass activity of 1.7×10^5 A·g$_{Ir}^{-1}$ and outstanding durability, maintaining operation at a current density of 1.8 A·cm^{-2} for 2700 h in a PEMWEs device. However, in less stable supports such as MnO_2 and Co_2MnO_4, atomically dispersed Ir species tend to reconstruct into aggregated IrO_x nanoparticles during electrochemical operation [64–66].

Yao et al. embedded Ru single atoms (Ru_1) into the Pt-rich coordination environment of $PtCu_x/Pt_{skin}$ core-shell nano-island chains to modify the electronic structure and redox behavior of Ru_1 through compressive strain of the Pt_{skin} shell (Fig. 3(a)) [67]. After acid etching and electrochemical leaching, the structure of Pt_xCu can be varied from Pt_3Cu, PtCu to Pt_3Cu periodic nano-islands with abundant defect sites, which could isolate Ru sites without forming Ru–O–Ru oxygen bridging bonds. As shown in Fig. 3(b), gradual release of surface compressive strain during acid etching and electrochemical leaching contributes to the shift of Ru d-band center closer to Femi level with optimized oxygen adsorption, presenting a typical inverse volcano plot. As shown in Fig. 3(c), Pt_3Cu also acts as an electron reservoir to donate electrons towards reaction intermediates and tailor the binding of oxygenated species close to an optimized level.

Carbon support, especially for N-doped carbon, could anchor

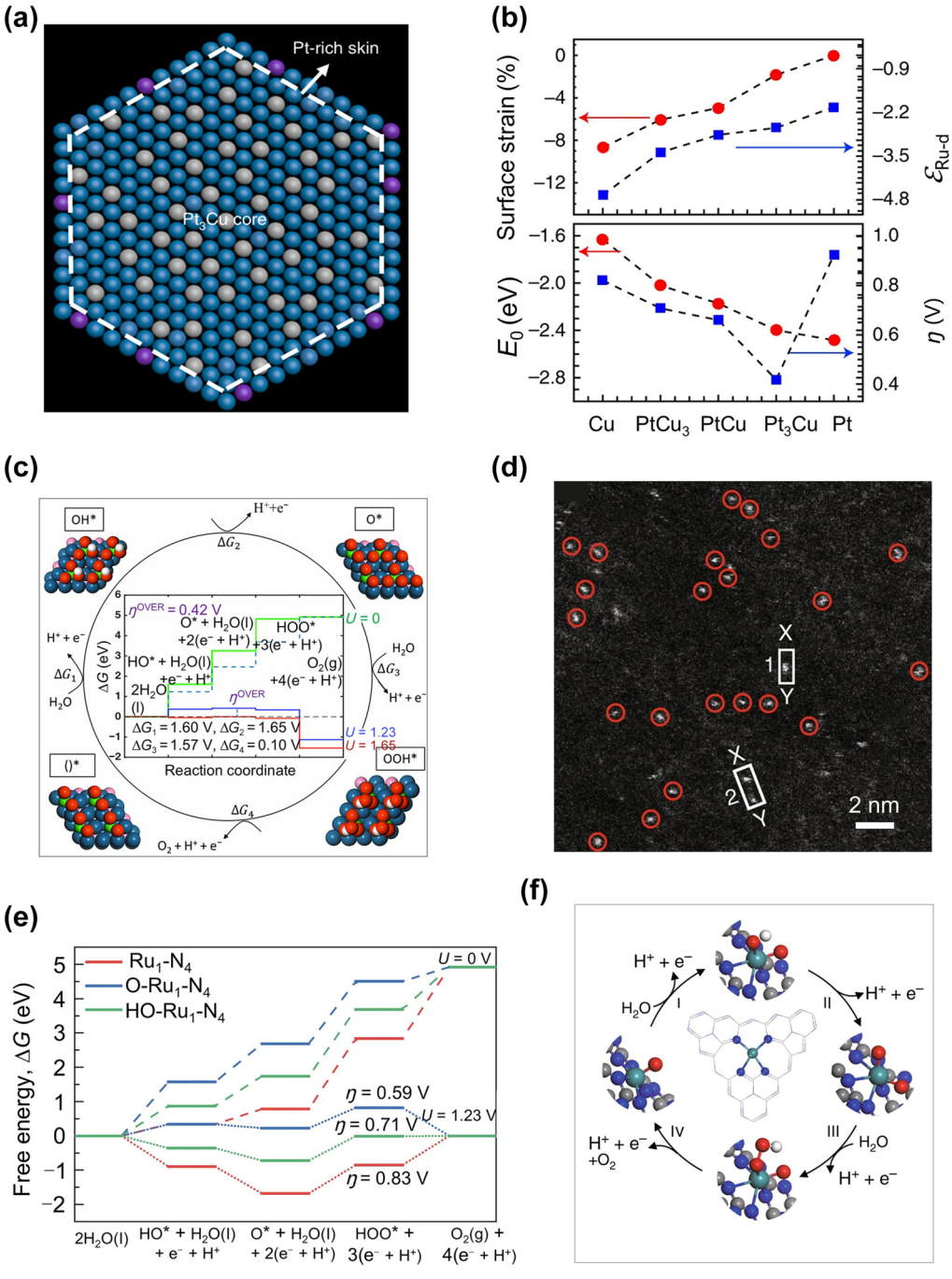

Figure 3 (a) Schematic atom model of Ru_1–Pt_3Cu, (b) In-plane lattice contraction relative to the Pt (111) pristine surface (red circles) and corresponding d-band centre ε_{Ru-d} of Ru_1 (blue squares), (c) OER mechanism and corresponding Gibbs free energy change and adsorption structures on Ru embedded Pt-skin Pt_3Cu (111). Reproduced with permission from Ref. [67], © Yao, Y. C. et al. 2019. (d) Magnified HAADF-STEM image of Ru-N-C form the highlighted area of Ru-N-C catalyst; (e) free energy diagram for OER on Ru_1-N_4 (red line), O-Ru_1-N_4 (blue line), and HO-Ru_1-N_4 (green line); (f) schematic of the whole OER mechanism on Ru-N-C catalyst in the acidic electrolyte. The balls in gray, blue, red, white, and light green represent C, N, O, H, and Ru atoms, respectively. Reproduced with permission from Ref. [68], © Cao, L. et al. 2019.

the metal atoms with abundant coordination structures and high loading. Besides, carbon support could create a single-atomic Ru with oxygen-free coordination in a conductive matrix to avoid the contribution of the LOER, which improves the dissolution resistance of APOEM. For example, a porphyrin-like Ru_1–N_4 structural configuration, with a mononuclear Ru coordinated with four N atoms, in carbon nitride-derived N–C support was designed as a robust and efficient APOEM (Fig. 3(d)). Under working conditions, after adsorption of O species, such O–Ru_1–N_4 site possesses a low barrier of O–O coupling to form the *OOH intermediates and thus boosts OER activity (Figs. 3(e) and 3(f)). With this trend, Ru–N–C exhibits superior performance in acid solution, achieving a current density of 10 mA cm^{-2} with a lower overpotential of 267 mV. However, the Ru–N–C catalysts can only maintain continuous operation for about 30 h in acid conditions [68]. Because thermodynamically unstable nature of carbon-based

materials at oxidation potential ($C_{(s)} + 2H_2O_{(l)} \rightarrow CO_{2(g)} + 4H^+ + 4e^-$ (0.207 vs. RHE)) directly leads to configuration collapse of APOEM and loss of active species, although the carbon skeleton plays a key role in dispersing and anchoring active sites. Not only are carbon materials not available to maintain steady performance during long-term catalysis under harsh acidic conditions, the over-oxidation of Ru to Ru–O_x moieties is believed to trigger another dissolution route, where active oxygen-coordinated Ru moieties peel off from defects [69].

SACs have garnered significant attention for AOER due to their high atomic utilization and tunable local coordination environments. However, their inherent isolated nature limits the exploitation of multi-site interactions and restricts the modulation of reaction pathways through cooperative effects. Specifically, single metal centers often face difficulty in simultaneously optimizing the adsorption energies of multiple reaction intermediates, a key limitation imposed by the scaling relationship in AOER. To overcome these constraints, researchers have begun to explore Multi-atom catalysts (MACs), where adjacent metal atoms, either homonuclear or heteronuclear, are anchored in proximity on a stable support.

To accurately embed multi-atom sites into the specific positions within the lattice of oxide supports, Shan et al. first reported the allocation of Ir atoms into the Co_3O_4 sublattice via an ion exchange procedure [70]. As shown in Figs. 4(a) and 4(b), the majority of Ir atoms occupy the Co_{oct} sites rather than the Co_{tet} sites in the spinel structure. Because of the spatial correlation between noble metal substitution sites and Co_3O_4 lattice, these noble metal single atoms show a short-range order and special Ir_{crs} topology with a 3D network composed of corner-shared tetrahedra. This arrangement eliminates the close-packing limitation in most metallic Ir phases that usually adopt an fcu or hcp topology through the oxygen-bridged noble metal arrangements (Fig. 4(c)).

A notable advancement by Lin et al. exploited a cation exchange strategy to synthesize Ru atom arrays supported on MnO_2 (Ru/MnO_2) satisfying the OPM criteria for AOER. In this way, the single Ru atoms inherited the periodicity of the MnO_2 support lattice, resulting in a lower interatomic distance of 2.9 than 3.1 Å in the original RuO_2 (Figs. 4(d) and 4(e)). Furthermore, the shortened distance and optimized electronic state of Ru atoms favor the coupling of O–O radicals (Figs. 4(f) and 4(g)) [52]. Beyond these structural criteria, minimizing noble metal consumption while maximizing atomic utilization has become essential in the current APOEM development [71].

Atomic-level regulatory strategies for APOEM: In the PEMWE system, the AOER has become a critical bottleneck restricting energy conversion efficiency due to its sluggish kinetics and the susceptibility of APOEM to corrosion. Therefore, the development of efficient and stable APOEM requires the implementation of precise regulation strategies to effectively address these challenges. To enhance its performance, atomic-level engineering control strategies involving multiple materials have been widely employed, such as defect engineering, interface engineering, strain engineering, and so on. These strategies are not mutually exclusive; instead, they often work synergistically, collectively addressing the trade-off between catalytic activity and stability, and providing multidimensional insights for the design of efficient and durable APOEM.

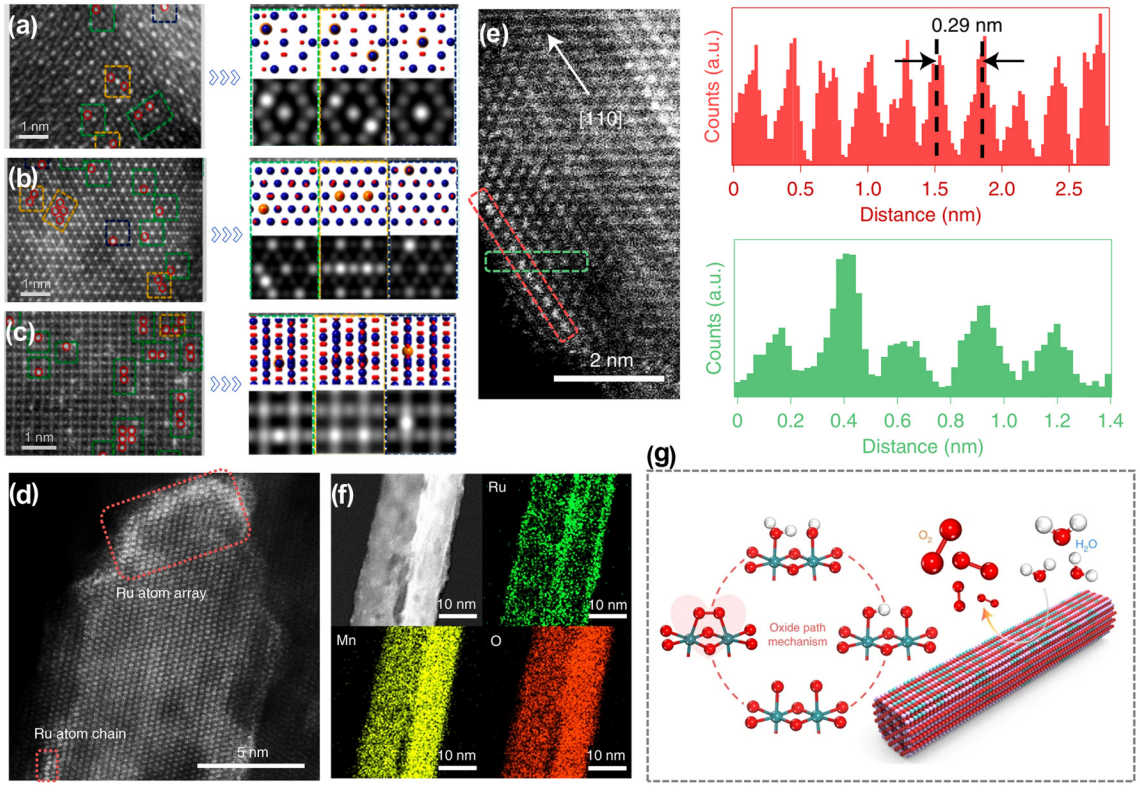

Figure 4 (a)–(c) HAADF-STEM images of Ir_{cru}-Co_3O_4 from diverse projections. The upper is structural projections and the lower is simulated projected Z^2-maps (Ir sites labeled by red circles). Reproduced with permission from Ref. [70], © American Chemical Society 2021. (d) Aberration-corrected HAADF-STEM image of the Ru/MnO_2 catalyst. The red dashed boxes present Ru atom chains or arrays. (e) The red and green dashed boxes show the ordered Ru atom arrangement on MnO_2. (f) EDS mapping images of the $12Ru/MnO_2$ catalyst and (g) schematics of OPM pathway for Ru/MnO_2 catalyst. Reproduced with permission from Ref. [52], © Lin, C. et al. 2021.

Defect engineering can optimize the electronic structure of the APOEM surface by introducing structural defects, such as vacancies and dislocations, which lead to the exposure of more active sites, a reduction in the reaction energy barrier, and enhanced adsorption compatibility with reaction intermediates. Grain boundaries (GBs) can induce structural defects, including vacancies, dislocations, and bond distortions, creating strained atomic coordination environments that modulate the electronic structures of active sites [72]. Densely packed GBs generate unsaturated coordination, tensile stresses, and high-energy surfaces that not only can regulate electronic configurations and intermediate adsorption energies but also provide anti-relaxation effects for improved AOER kinetics and stability. Grain boundaries engineering strategy shows potential to resolve the persistent activity-stability trade-off in RuO_2-based APOEM. Wang and co-workers fabricated a grain boundary-engineered RuO_2 catalyst (GB-RuO_2) as ultrathin porous nanosheets [73]. GBs induced tensile stress and unsaturated coordination, optimizing intermediate adsorption and stabilizing active sites during AOER.

Interface engineering can enhance electrocatalytic activity in hybrid nanomaterials through synergistic dual/multi-active site effects [74–76]. Rational heterostructure design enables spatially proximate reaction steps across distinct active components, accelerating overall kinetics. This coupling further modulates electronic states, as exemplified by Mott–Schottky effects at Janus metal-semiconductor interfaces, facilitating rapid multi-electron transfer. A recent study has demonstrated that Ni ions contribute to the activation of neighboring inert manganese atoms on manganese octahedral molecular sieves (OMS) with Ru-Mn pair as shown in Fig. 5(a). The tunnel Ni ions acted as dynamic electron donors and acceptors, promoting accelerated deprotonation of Mn at specific sites. Simultaneously, they contribute to structural stabilization through the formation of O–Ru^{IV}–O–Mn^{IV}–O interactions and the reinforcement of Mn–O bonds (Fig. 5(b)). Besides, Ni ions are effective tunnel fillers to preserve OMS connectivity by preventing a cross-site disproportionation of Mn^{3+} in acidic solutions [77].

Recently, the core–shell structure of Ru@RuO_2 (CoRu@RuO_2) catalysts with integrated atoms has been developed. The

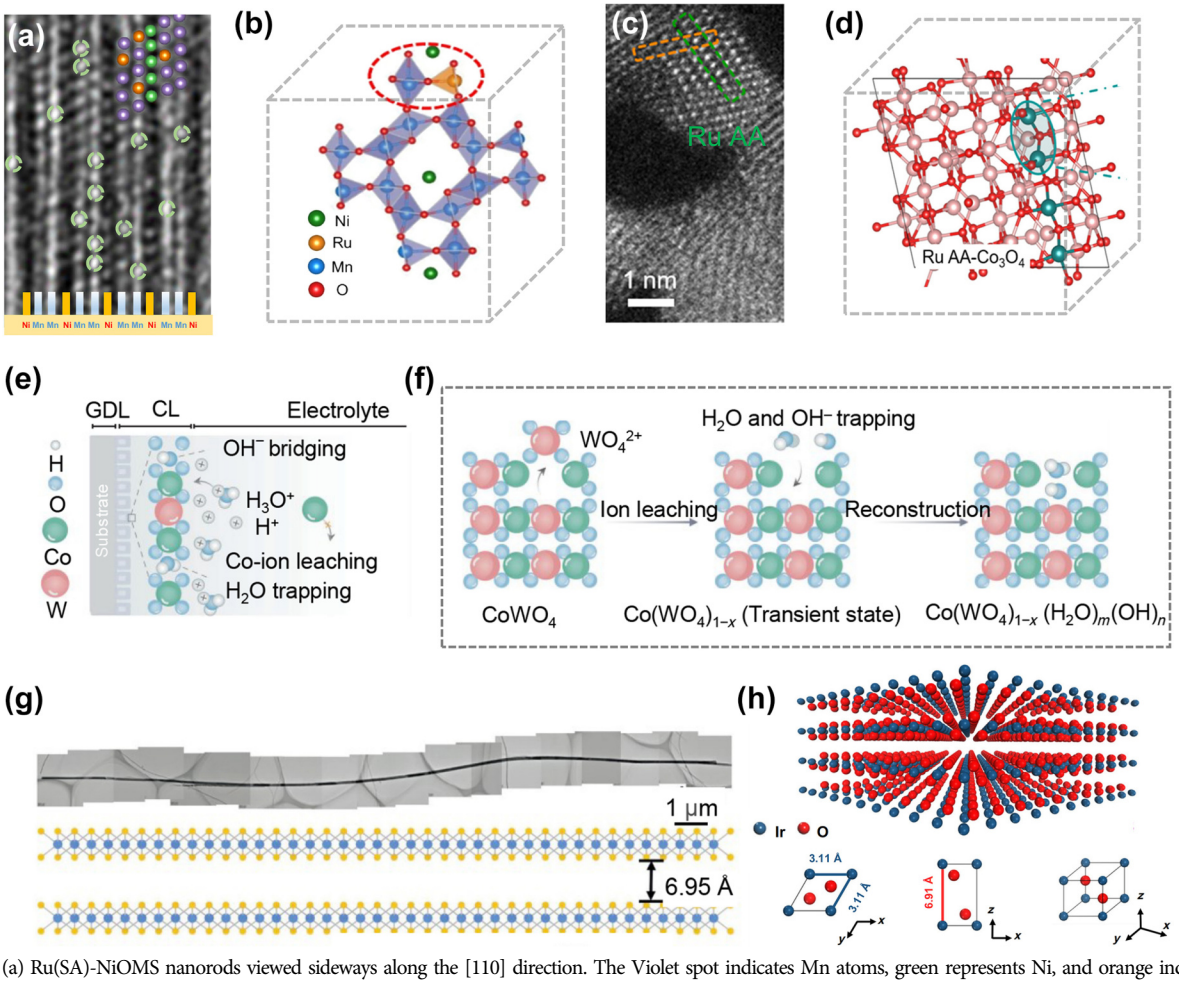

Figure 5 (a) Ru(SA)-NiOMS nanorods viewed sideways along the [110] direction. The Violet spot indicates Mn atoms, green represents Ni, and orange indicates Ru atoms; (b) Structure models of $Ru_{(SA)}$-NiOMS from the top view. Reproduced with permission from Ref. [77], © Hao, Y. et al. 2024. (c) HAADF-STEM image of Ru_{AA}-Co_3O_4; (d) The structure model of Ru_{AA}-Co_3O_4; The green and orange dashed boxes demonstrate the distribution of Ru atoms and Co atoms arrangement in the Co_3O_4 lattice. Reproduced with permission from Ref. [51], © American Chemical Society 2024. (e) Schematic illustration of the dissolution of Co ions in Co_3O_4 through Co–O bond cleaving, followed by their hydration in acidic medium. (f) A depiction of delaminated cobalt catalysts (CWO-del-48), illustrating the effect of water trapping and hydroxide bridging within the crystal lattice, enabling stability in acid. Reproduced with permission from Ref. [83], © Ram, R. et al. 2024. (g) A typical long IrO_2 NR with a length of 22.53 μm; (h) Atomic structure of layered 1T-IrO_2. Schematic of the unit cell of 1T-IrO_2 with the lattice constants of $a = b = 3.11$ Å and $c = 6.91$ Å. The refined structure models are obtained based on the XRD and the aberration corrected HAADF-STEM analysis. Ir and O are represented by blue and red spheres, respectively. Reproduced with permission from Ref. [89], © Fan, Z. L.et al. 2021.

metal–metal oxide core–shell architecture enhances the stability of Ru-based APOEM, achieving a low overpotential of 203 mV and excellent stability over a 400-hour durability test at 10 mA·cm^{-2} [78]. Cao and co-workers developed a core-shell RuCo/RuCoO$_x$ structure with confined Schottky heterojunctions via controlled oxidation of RuCo alloys [79]. This design maximizes active site accessibility while enhancing durability and intrinsic AOER activity. Schottky-induced lattice strain and charge transfer modulate electronic structures, suppressing Ru over-oxidation/dissolution and protecting the metallic RuCo core from acid corrosion. Wang reported a controlled metallic Ru deposition strategy on RuO$_2$ surfaces to construct Ru^{4+}–O–Ru^0 interfaces [80]. Metallic Ru acts as an electron donor, reducing *V$_O$–RuO$_4^{2-}$ oxidation states in Ru/RuO$_2$ and stabilizing its structure for enhanced AOER stability. Concurrently, Ru^{4+}–Ru^0 interfacial oxygen sites accelerate deprotonation kinetics, boosting AOER activity.

The emergence of ordered atomic arrays offers a new horizon for the design of APOEM. Ru atomic arrays on Co$_3$O$_4$ (Ru$_{AA}$-Co$_3$O$_4$) electrocatalyst avoided the participation of lattice O and then achieved direct O* radical coupling to produce O$_2$. Because Ru atoms adopted the periodic atomic arrangement guided by the Co$_3$O$_4$ lattice, the interatomic distance of symmetric Ru–Ru sites were shortened from 3.1 to 2.5 Å. The optimized Ru atom distance enabled direct O* coupling, as confirmed by electrochemical attenuated total reflectance surface-enhanced IR spectroscopy. Enabled by the favorable OPM pathway, the Ru$_{AA}$-Co$_3$O$_4$ electrocatalyst delivered a 160 mV overpotential and a high TOF value of 7.7 s^{-1} at E_{j10} in 0.5 M H$_2$SO$_4$, increasing the intrinsic activity and the utilization efficiency of Ru (Figs. 5(c) and 5(d)) [51]. Rational spatial organization of active sites can favor optimal reaction pathways with maximizing atomic efficiency, ultimately leading to exceptional catalytic performance [81].

Strain engineering modifies atomic spacing through lattice stretching or compression, adjusts the position of the d-band center, and optimizes the bonding strength between active sites and reactant molecules, thereby improving catalytic performance. Chen et al. developed a single-atom cobalt-doped core–shell heterostructure catalyst, denoted as Co–Ru@RuO$_2$, consisting of a metallic Ru core and a RuO$_2$ shell. In this structure, lattice contraction within the RuO$_2$ shell primarily arises from two factors: the lattice parameter mismatch between the Ru core and the RuO$_2$ shell, and the incorporation of Co atoms, which have a smaller atomic radius, into the RuO$_2$ lattice [82]. This compressive strain results in a downward shift of the d-band center of surface Ru atoms relative to the Fermi level, effectively reducing their electron density. Consequently, the adsorption strength of oxygen-containing intermediates at the Ru active sites is weakened.

Component regulation modifies the electronic structure of a catalyst through alloying, doping, and related methods. For instance, introducing highly electronegative elements can enhance the oxidation capability of the metal center, thereby improving the intrinsic catalytic activity. Ram and co-workers demonstrated that the enhanced control over the AOER mechanism involving only *O and *OH as intermediates by proposed a structural delamination strategy, whereby high valence sacrificial tungsten (W) elements in a CoWO$_4$ (CWO) crystal structure be selective removal through a water-hydroxide-WO$_4^{2-}$ anion exchange process (Figs. 5(e) and 5(f)) [83]. This structural delamination provides a Co oxide defect network to trap and stabilize water and hydroxide species. As a result, the Co ion dissolution in acid shows a marked decrease in CWO compared with Co$_3$O$_4$ due to the water-hydroxide shielding renders. Encouraged by the stabilization of oxide and water-hydroxide networks, the CWO lattice delaminated (CWO-del) catalysts exhibit excellent cell performance in PEMWEs system under industrial operational settings, which achieving a current density of 1.8 A·cm^{-2} at 2 V and stable operation for 608 h at 1 A·cm^{-2} with a cell voltage of 1.77 V.

Doping has emerged as one of the most widely studied modification strategies for Ru-based APOEM [84–86], as it can enhance APOEM stability without compromising the apparent AOER activity of RuO$_2$. A growing number of works have demonstrated that doping can effectively tune the electronic structure of RuO$_2$, modulate the dynamic changes in Ru oxidation states during AOER, accelerate proton-coupled electron transfer steps, and optimize the adsorption energies of key OER intermediates. Kang and co-workers achieved enhanced intrinsic AOER activity and suppressed corrosion of RuO$_2$ through Ta doping [87]. Ta incorporation effectively suppressed the transformation of Ru sites into unstable high-valent intermediates during AOER, significantly reducing Ru dissolution while mitigating surface degradation through inhibited cluster exsolution and reconstruction.

Rutile IrO$_2$ can be transformed into layered A$_x$Ir$_y$O$_z$ compounds via the intercalation of alkali metal ions (A$^+$) and subsequent phase transformation [88]. These layered intermediates can then be exfoliated into two-dimensional IrO$_2$ nanosheets with a hexagonal lattice through acid treatment and cation exchange (e.g., with tetrabutylammonium ions). By further optimizing this synthetic strategy, such as selecting different Ir precursors (e.g., IrO$_2$, IrCl$_3$, or Ir(acac)$_3$), varying the alkali metal sources (e.g., alkali metal carbonates or hydroxides), and tuning the reaction temperature, various metastable IrO$_2$ phases have been successfully obtained, including 1T-IrO$_2$ (Figs. 5(g) and 5(h)), 3R-IrO$_2$, monoclinic IrO$_2$, and amorphous IrO$_x$ nanosheets [89]. These low-dimensional Ir-based structures exhibit significantly enhanced intrinsic activity compared to bulk IrO$_2$. Their implementation in membrane electrode assemblies enables low loading while maximizing Ir utilization. Moreover, their favorable porous architectures facilitate efficient mass transport, including the release of oxygen bubbles and the delivery of water [90]. Additionally, the metastable structures offer valuable insights into the relationship between structural motifs and AOER activity, shedding light on how atomic arrangement influences catalytic performance.

AI-accelerated development of advanced APOEM: The traditional ETAE approach has accumulated valuable experience for the design of APOEM. Data-driven APOEM design powered by AI technologies is emerging as a focal point of research, offering significant advantages in component optimization, structural screening, and the prediction of structure–activity relationships [91]. By integrating ML algorithms with high-throughput computational and automated robotic platforms, researchers can efficiently navigate the vast design space of catalytic materials. Moreover, AI-assisted models can identify hidden patterns and correlations within complex datasets, enabling the rational design of APOEM with tailored properties. As a result, the synergy between AI and traditional ETAE methods is expected to drive the next generation of breakthroughs in APOEM development. As these techniques mature, the synergy between AI-driven predictions and mechanistic understanding will further facilitate the rational control of active site geometry, electronic environment, and atomic

arrangement, offering new momentum for the design of next-generation APOEM. Recent studies have demonstrated the ability of AI algorithms to capture nonlinear correlations among geometric, electronic, and kinetic descriptors, thereby guiding the targeted synthesis of advanced materials. Moreover, the integration of active learning loops with DFT calculations and automated synthesis platforms enables closed-loop APOEM design, significantly reducing development time.

By training ML models, specific features (e.g., d-band center, electronegativity, and valence electron count) are identified and correlated with either intermediate binding energies or experimental activity metrics [92, 93]. This process enables the discovery of meaningful descriptors that underlie and potentially predict catalytic performance. Gong and co-workers employed high-throughput DFT calculations to develop an interpretable descriptor model for predicting activity and selectivity across multiple electrocatalytic reactions, including OER [94]. The model decouples atomic, reactant, synergistic, and coordination effects on the d-band shape of dual-atom sites, based on physically meaningful feature engineering (Fig. 6(a)). A combined DFT–ML framework was employed to predict adsorption energies across hundreds of multi active centers candidates. For structural screening, Li and co-workers presented a closed-loop framework that predicted $RbSbWO_6$ as a promising bifunctional APOEM. Bulk Pourbaix

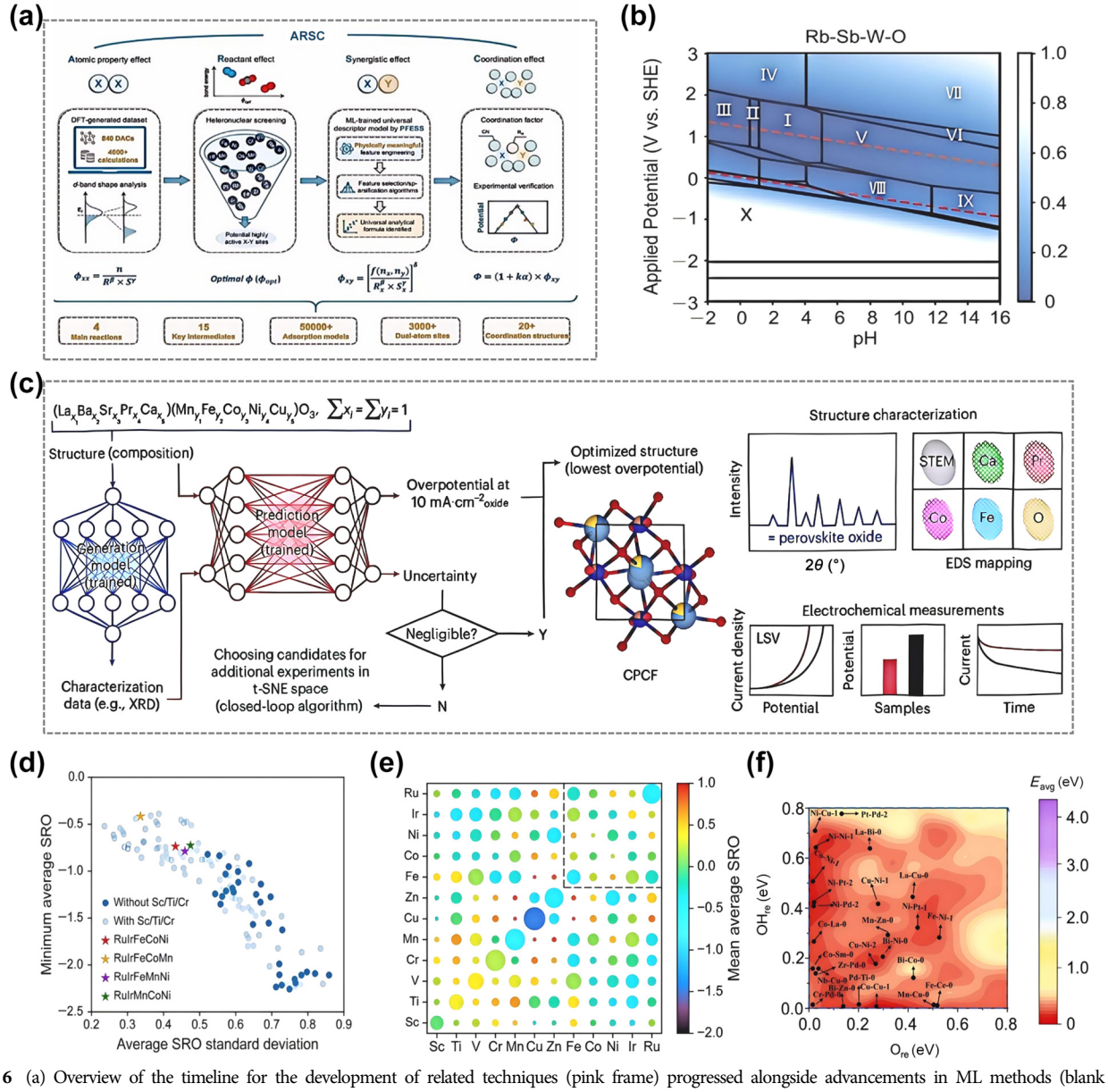

Figure 6 (a) Overview of the timeline for the development of related techniques (pink frame) progressed alongside advancements in ML methods (blank text). Reproduced with permission from Ref. [94], © Lin, X. Y. et al. 2024. (b) Bulk Pourbaix diagram of Rb–Sb–W–O system. Reproduced with permission from Ref. [95], © American Chemical Society 2025. (c) The red (prediction) model and the blue (generation) model are individually trained for the screening process, and the predicted optimal oxide is synthesized and undergoes structure characterization and electrochemical performance verification. Reproduced with permission from Ref. [96], © Li, X. Y. et al. 2024. (d) Scatter plot of the minimum average SRO vs the standard deviation of average SRO and (e) correlation plot of the mean (indicated by circle color) and standard deviation (indicated by circle radius) of the average SRO. Reproduced with permission from Ref. [97], © American Chemical Society 2025. (f) Heat map of the predicted E_{avg} of different double-atom/cluster APOEM, confirming that machine learning approaches can efficiently navigate the vast compositional space to pinpoint stable and active dual-atom sites. Reproduced with permission from Ref. [98], © Luo, Y. et al. 2023.

diagrams further indicated its exceptional stability under acidic conditions within the applied OER potential range (Fig. 6(b)) [95].

The integrated experimental platform validated the prediction and demonstrated the stable operation of $RbSbWO_6$-based heterostructured electrocatalysts in a PEMWE system for 120 h at a current density of 500 mA·cm^{-2}. For compositional optimization, AI-driven design offers the advantage of high-throughput screening. The composition of multi-metal oxides, including perovskite oxides, can be effectively optimized through active learning with small datasets, informative structural characterization data, and integrated into closed-loop experimental workflows (Fig. 6(c)) [96]. The composition of Ru-based multicomponent alloys was optimized by a machine-learned interatomic potential coupled with replica-exchange molecular dynamics (Figs. 6(d) and 6(e)) [97]. To bridge the gap between theoretical atomic design and practical implementation, specific artificial intelligence (AI) methodologies play a crucial role in guiding the atomic-level engineering strategies discussed in the preceding sections. Firstly, ML Potentials have emerged as a potent instrument to tackle the challenges in interface and cluster engineering. In contrast to traditional DFT, which is restricted to small systems, ML potentials enable high-accuracy simulations of large-scale atomic arrays and complex solid-liquid interfaces [89]. This ability is essential for validating the dynamic stability of the OPM pathway in multi-atom ensembles under acidic conditions. Secondly, active learning frameworks are essential for component regulation and doping. Through iterative selection of the most informative experiments, AL can effectively screen the extensive combinatorial space of high-entropy alloys or multi-doped oxides [88], and promptly identify the optimal compositions that balance the activity-stability trade-off. Ultimately, AI-driven inverse design approaches can directly guide Strain and Defect Engineering. Instead of the trial-and-error adjustment of lattice parameters, machine learning models can predict the precise lattice strain required for optimizing the d-band center, thereby determining the exact synthesis conditions needed to achieve the desired electronic structure.

Atomic and structural descriptors (including metal identity and active site configuration) were used to represent multi active centers systems. This approach identified 10 multi active centers catalysts with OER activity exceeding that of the RuO_2 (Fig. 6(f)) [98]. These acceleration strategies further enhance the design of advanced Ir-based, Ru-based, and non-precious metals-based APOEM. Table S1 in the Electronic Supplementary Material (ESM) lists the progress and data of typical catalysts over the past three years. A statistical analysis of the performance data in Table S1 in the ESM reveals distinct trends regarding the stability of APOEMs governed by different mechanisms. Generally, catalysts following the AEM pathway (mostly isolated single-atom catalysts) tend to exhibit limited durability, often operating for less than 100 h, likely due to the vulnerability of isolated sites to dynamic restructuring or support corrosion. In contrast, materials engineered to follow LOM or OPM pathways demonstrate significantly enhanced longevity. Notably, OPM-based catalysts, such as short-range ordered Ru atom arrays, achieve exceptional stability exceeding 1000 h (e.g., 1500 h for Ru array-Co_3O_4 and 1050 h for Vn-RuO_2). This trend empirically supports the design philosophy that facilitating direct O–O radical coupling (OPM) or stabilizing lattice oxygen (optimized LOM) is crucial for overcoming the intrinsic activity-stability trade-off in acidic environments. The majority of the currently reported high-performance APOEMs still adhere to the AEM or LOM pathways. This disparity between the theoretical advantage of OPM and its practical paucity mainly results from synthetic challenges. Unlike AEM or LOM, the implementation of OPM necessitates the accurate construction of dual-metal active sites with stringent interatomic spacing constraints to facilitate direct O–O radical coupling. Attaining such atomic-level precision is challenging through traditional trial-and-error approaches. This emphasizes that although OPM materials are more challenging to fabricate, they represent a crucial direction for overcoming the activity-stability trade-off, a task that AI-driven intelligent manufacturing (ADIM) is well-suited to expedite.

Looking ahead, the continued integration of AI with experimental and theoretical catalysis holds great promise for revolutionizing APOEM design. As more high-quality datasets become available and ML models grow increasingly sophisticated, we can expect more accurate predictions and deeper insights into catalytic behavior at the atomic scale [99]. By integrating advanced ML models, researchers can more effectively navigate the vast design space of APOEM. This synergy enables the rapid identification of optimal coordination environments, electronic structures, and reaction energetics tailored to specific OER mechanisms. Ultimately, this interdisciplinary approach will not only expedite the discovery of efficient and stable catalysts but also contribute to the broader goal of achieving sustainable and scalable hydrogen production through advanced water electrolysis technologies.

6 Conclusions and perspective

The AOER plays a vital role in various electrochemical and energy-related technologies, particularly in PEMWEs. PEMWEs are the core devices for green hydrogen production, so APOEM performance directly influences the efficiency of green hydrogen synthesis. The goal of APOEM is to precisely control the arrangement of atoms, which in turn enables the achievement of desired catalytic performance. To accelerate reaction kinetics, it is necessary to develop advanced APOEM. These catalysts are specifically APOEM and they need to have uniformly well-defined structures, periodic atomic arrangements, favorable active site configurations, and optimized adsorption energies for reaction intermediates. Such precise and high-performance features are difficult to achieve through traditional ETAE approaches, as these methods often lack precision and efficiency in material design. A comprehensive and integrated roadmap is essential (Fig. 7). This roadmap goes beyond conventional ETAE methods by synergizing four critical dimensions from ETAE to ADIM. The second is the application of advanced *in-situ* characterization techniques, which helps gain deep mechanistic insights into AOER processes. The third is the integration of AI with high-throughput computing, a combination that can predict optimal APOEM configurations accurately. The fourth dimension is the adoption of robotic synthesis, which enables the realization of ADIM. The details of these strategies are provided in the following four sections.

(1) Rational design of ordered active sites for stability and cost efficiency: To achieve the goal of the APOEM design, research must focus on minimizing the usage of Ir-/Ru-based materials without compromising catalytic performance. By optimizing the electronic structure of every atomic site and increasing atomic load density, the ordered atomic sites can tune the local electrical structure and maximize synergistic effects. This multi-site design strategy is essential for creating robust APOEM that excel in both activity and

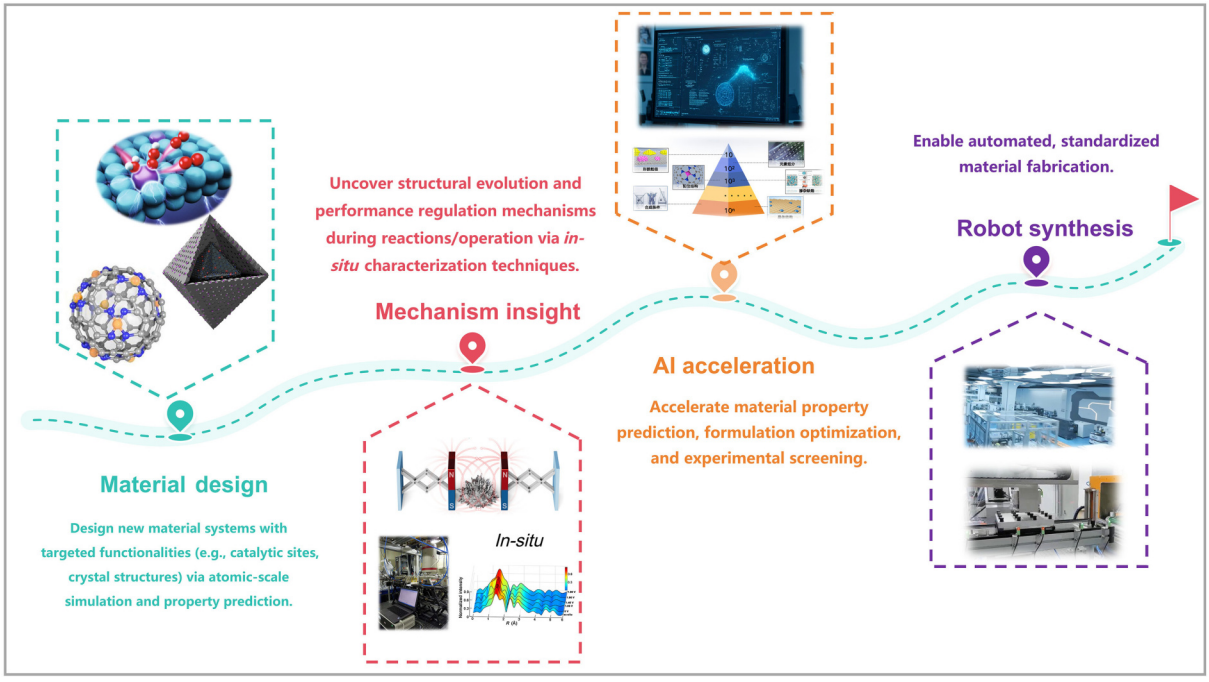

Figure 7 Roadmap for accelerated APOEM discovery. This comprehensive framework integrates rational design, *in-situ* characterization, AI acceleration, and robotic synthesis to achieve a closed-loop autonomous discovery of next-generation catalysts.

stability at industry-level current densities, addressing challenges such as impeded ion transport and active site degradation in PEMWEs.

(2) Uncovering dynamic evolution via advanced *in-situ* characterization: Deep conceptual insight into the reaction mechanism is a prerequisite for rational design. There is a pressing need to develop more accurate characterization techniques to capture the dynamic data of the catalytic surface, including structural evolution and electron transport. Rather than relying solely on average results from X-ray absorption spectroscopy, researchers should utilize aberration-corrected STEM to identify local coordination environments and atomic distributions. Furthermore, investigating the *in-situ* evolution of devices under realistic operating conditions using advanced electrochemical spectroscopies will provide a comprehensive view of reaction pathways and help elucidate the origins of stability, particularly for Ru-based APOEM.

(3) Paradigm shift from ETAE to ADIM: Facing the vast combinatorial space of APOEM, traditional ETAE approaches are inefficient. The integration of AI and ML is revolutionizing this process by shifting to a data-driven methodology. High-throughput screening and density functional theory provide high-quality training datasets, enabling the systematic prediction of crystal structures, electronic properties, and performance metrics like adsorption free energy. This capability allows for the rapid screening of potential candidate materials and efficient formulation optimization, significantly accelerating the discovery of efficient and economical APOEM.

(4) Enabling Automated Fabrication and Autonomous Discovery: To bridge the gap between laboratory research and industrial application, controlled synthesis methods must be scaled up to manufacturing levels. While approaches like impregnation and vapor deposition show promise for commercial-scale production, the future lies in achieving a fully automated system. By integrating robot automation platforms, the field can realize a standardized process covering theoretical prediction, material synthesis, and performance testing.

In summary, the future of APOEM advancement depends on the seamless integration of these four pivotal strategies: rational material design, mechanistic insight, AI acceleration, and robotic synthesis. This rational design must be continuously informed by advanced *in-situ* characterization techniques that reveal real-time structural evolution and reaction dynamics, ensuring that theoretical models align with practical operational realities. Furthermore, the convergence of AI with robotic automation represents a transformative leap toward a closed-loop, autonomous discovery system. This synergy not only expedites the screening of vast material spaces but also guarantees the standardized, reproducible fabrication necessary for industrial scalability. Ultimately, realizing this holistic roadmap will bridge the divide between laboratory innovation and commercial application, unlocking the full potential of PEMWEs and paving the way for a sustainable, cost-effective global hydrogen economy.

Electronic Supplementary Material: Supplementary Material is available in the online version of this article at https://doi.org/10.26599/NR.2026.94908378.

Data availability

All data needed to support the conclusions in the paper are presented in the manuscript and the Electronic Supplementary Material. Additional data related to this paper may be requested from the corresponding author upon request.

Acknowledgements

This work was supported by China Ministry of Science and Technology (No. 2020YFA0710203), the Major Frontier Research Project of the University of Science and Technology of China (No.

LS2060000002), the Joint Funds of the National Natural Science Foundation of China (No. U23A2081), the National Natural Science Foundation of China (No. 22221003), the Anhui Provincial Key Research and Development Project (No. 2023z04020010), the Anhui Provincial Natural Science Foundation (Nos. 2108085UD06 and 2208085UD04), USTC Research Funds of the Double First-Class Initiative (No. YD2060006005), and Start-up Funding of the University of Science and Technology of China (No. KY2490000003).

Declaration of competing interest

All the contributing authors report no conflict of interests in this work.

Author contribution statement

Y. X.: Writing – original draft, formal analysis, investigation, data curation, validation. B. W.: Writing – original draft, formal analysis. W. Z. L.: Writing – original draft, investigation, validation. J. N. L.: Formal analysis, investigation. X. R. R.: Formal analysis, investigation. C. Q.: Investigation, resources. X. G. Y.: Investigation, resources. J. C. S.: Investigation, resources. H. Z.: Project administration, supervision. Y. F. Z.: Conceptualization, writing – review & editing, supervision. Y. E. W.: Supervision, funding acquisition. All the authors have approved the final manuscript.

Use of AI statement

None.

References

[1] Li, R. Z.; Zhao, J.; Liu, B. Z.; Wang, D. S. Atomic distance engineering in metal catalysts to regulate catalytic performance. *Adv. Mater.* **2024**, *36*, 2308653.

[2] Carmo, M.; Fritz, D. L.; Mergel, J.; Stolten, D. A comprehensive review on PEM water electrolysis. *Int. J. Hydrogen Energy* **2013**, *38*, 4901–4934.

[3] Lagadec, M. F.; Grimaud, A. Water electrolysers with closed and open electrochemical systems. *Nat. Mater.* **2020**, *19*, 1140–1150.

[4] Ni, J.; Shi, Z. P.; Wang, X.; Wang, Y. B.; Wu, H. X.; Liu, C. P.; Ge, J. J.; Xing, W. Recent development of low iridium electrocatalysts toward efficient water oxidation. *J. Electrochem.* **2022**, *28*, 2214010.

[5] Chen, X. J.; Liao, W. Y.; Zhong, M. X.; Chen, J. J.; Yan, S.; Li, W. M.; Wang, C.; Chen, W.; Lu, X. F. Rational design of robust iridium-ceria oxide-carbon nanofibers to boost oxygen evolution reaction in both alkaline and acidic media. *Nano Res.* **2023**, *16*, 7724–7732.

[6] Zhao, G. Q.; Luo, Z. X.; Zhang, B. H.; Chen, Y. P.; Cui, X. Z.; Chen, J.; Liu, Y. F.; Gao, M. X.; Pan, H. G.; Sun, W. P. Epitaxial interface stabilizing iridium dioxide toward the oxygen evolution reaction under high working potentials. *Nano Res.* **2023**, *16*, 4767–4774.

[7] Liu, Z. J.; Wang, G. J.; Guo, J. Y.; Wang, S. Y.; Zang, S. Q. Sub-2 nm IrO_2/Ir nanoclusters with compressive strain and metal vacancies boost water oxidation in acid. *Nano Res.* **2023**, *16*, 334–342.

[8] Hao, S. Y.; Sheng, H. Y.; Liu, M.; Huang, J. Z.; Zheng, G. K.; Zhang, F.; Liu, X. N.; Su, Z. W.; Hu, J. J.; Qian, Y. et al. Torsion strained iridium oxide for efficient acidic water oxidation in proton exchange membrane electrolyzers. *Nat. Nanotechnol.* **2021**, *16*, 1371–1377.

[9] Ji, M. W.; Yang, X.; Chang, S. D.; Chen, W. X.; Wang, J.; He, D. S.; Hu, Y.; Deng, Q.; Sun, Y.; Li, B. RuO_2 clusters derived from bulk $SrRuO_3$: Robust catalyst for oxygen evolution reaction in acid. *Nano Res.* **2022**, *15*, 1959–1965.

[10] Mefford, J. T.; Rong, X.; Abakumov, A. M.; Hardin, W. G.; Dai, S.; Kolpak, A. M.; Johnston, K. P.; Stevenson, K. J. Water electrolysis on $La_{1-x}Sr_xCoO_{3-\delta}$ perovskite electrocatalysts. *Nat. Commun.* **2016**, *7*, 11053.

[11] Kibsgaard, J.; Chorkendorff, I. Considerations for the scaling-up of water splitting catalysts. *Nat. Energy* **2019**, *4*, 430–433.

[12] Wang, Y.; Zheng, X. B.; Wang, D. S. Design concept for electrocatalysts. *Nano Res.* **2022**, *15*, 1730–1752.

[13] Chen, F. Y.; Wu, Z. Y.; Adler, Z.; Wang, H. T. Stability challenges of electrocatalytic oxygen evolution reaction: From mechanistic understanding to reactor design. *Joule* **2021**, *5*, 1704–1731.

[14] Nie, L.; Mei, D. H.; Xiong, H. F.; Peng, B.; Ren, Z. B.; Hernandez, X. I. P.; DeLaRiva, A.; Wang, M.; Engelhard, M. H.; Kovarik, L. et al. Activation of surface lattice oxygen in single-atom Pt/CeO_2 for low-temperature CO oxidation. *Science* **2017**, *358*, 1419–1423.

[15] Gunasooriya, G. T. K. K.; Nørskov, J. K. Analysis of acid-stable and active oxides for the oxygen evolution reaction. *ACS Energy Lett.* **2020**, *5*, 3778–3787.

[16] Zheng, X. B.; Yang, J. R.; Xu, Z. F.; Wang, Q. S.; Wu, J. B.; Zhang, E. H.; Dou, S. X.; Sun, W. P.; Wang, D. S.; Li, Y. D. Ru–Co pair sites catalyst boosts the energetics for the oxygen evolution reaction. *Angew. Chem., Int. Ed.* **2022**, *61*, e202205946.

[17] Wen, Y. Z.; Chen, P. N.; Wang, L.; Li, S. Y.; Wang, Z. Y.; Abed, J.; Mao, X. N.; Min, Y. M.; Dinh, C. T.; De Luna, P. et al. Stabilizing highly active Ru sites by suppressing lattice oxygen participation in acidic water oxidation. *J. Am. Chem. Soc.* **2021**, *143*, 6482–6490.

[18] Jin, H. Y.; Liu, X. Y.; An, P. F.; Tang, C.; Yu, H. M.; Zhang, Q. H.; Peng, H. J.; Gu, L.; Zheng, Y.; Song, T. et al. Dynamic rhenium dopant boosts ruthenium oxide for durable oxygen evolution. *Nat. Commun.* **2023**, *14*, 354.

[19] Zhou, Y. N.; Chen, L. L.; Sheng, L.; Luo, Q. Q.; Zhang, W. H.; Yang, J. L. Dual-metal atoms embedded into two-dimensional covalent organic framework as efficient electrocatalysts for oxygen evolution reaction: A DFT study. *Nano Res.* **2022**, *15*, 7994–8000.

[20] Wei, B.; Fu, Z. H.; Legut, D.; Germann, T. C.; Du, S. Y.; Zhang, H. J.; Francisco, J. S.; Zhang, R. F. Rational design of highly stable and active MXene-based bifunctional ORR/OER double-atom catalysts. *Adv. Mater.* **2021**, *33*, 2102595.

[21] Chen, R. Z.; Chen, S. H.; Wang, L. Q.; Wang, D. S. Nanoscale metal particle modified single-atom catalyst: Synthesis, characterization, and application. *Adv. Mater.* **2024**, *36*, 2304713.

[22] Huang, Z. F.; Xi, S. B.; Song, J. J.; Dou, S.; Li, X. G.; Du, Y. H.; Diao, C. Z.; Xu, Z. J.; Wang, X. Tuning of lattice oxygen reactivity and scaling relation to construct better oxygen evolution electrocatalyst. *Nat. Commun.* **2021**, *12*, 3992.

[23] Zhao, Y. F.; Guo, Y.; Lu, X. F.; Luan, D. Y.; Gu, X. J.; Lou, X. W. Exposing single Ni atoms in hollow S/N-doped carbon macroporous fibers for highly efficient electrochemical oxygen evolution. *Adv. Mater.* **2022**, *34*, 2203442.

[24] Zhao, Y. F.; Lu, X. F.; Fan, G. L.; Luan, D. Y.; Gu, X. J.; Lou, X. W. Surface-exposed single-Ni atoms with potential-driven dynamic behaviors for highly efficient electrocatalytic oxygen evolution. *Angew. Chem., Int. Ed.* **2022**, *61*, e202212542.

[25] Song, J. J.; Wei, C.; Huang, Z. F.; Liu, C. T.; Zeng, L.; Wang, X.; Xu, Z. J. A review on fundamentals for designing oxygen evolution electrocatalysts. *Chem. Soc. Rev.* **2020**, *49*, 2196–2214.

[26] Zhao, Y. F.; Zhou, H.; Zhu, X. R.; Qu, Y. T.; Xiong, C.; Xue, Z. G.; Zhang, Q. W.; Liu, X. K.; Zhou, F. Y.; Mou, X. M. et al. Simultaneous oxidative and reductive reactions in one system by atomic design. *Nat. Catal.* **2021**, *4*, 134–143.

[27] Wei, Y. S.; Sun, L. M.; Wang, M.; Hong, J. H.; Zou, L. L.; Liu, H. W.; Wang, Y.; Zhang, M.; Liu, Z.; Li, Y. W. et al. Fabricating dual-atom iron catalysts for efficient oxygen evolution reaction: A heteroatom modulator approach. *Angew. Chem., Int. Ed.* **2020**, *59*, 16013–16022.

[28] Hardisty, S. S.; Lin, X. Q.; Kucernak, A. R. J.; Zitoun, D. Single-atom Pt on carbon nanotubes for selective electrocatalysis. *Carbon Energy* **2024**, *6*, e409.

[29] Zhou, Y. N.; Sheng, L.; Chen, L. L.; Zhao, W. H.; Zhang, W. H.; Yang, J. L. Metal and ligand modification modulates the electrocatalytic HER, OER, and ORR activity of 2D conductive metal-organic frameworks. *Nano Res.* **2024**, *17*, 7984–7990.

[30] Xiao, L. Y.; Bai, X.; Han, J. Y.; Tang, T. M.; Chen, S. Y.; Qi, H.; Hou, C. M.; Bai, F. Q.; Wang, Z. L.; Guan, J. Q. Surface reconstruction and structural transformation of two-dimensional Ni–Fe MOFs for oxygen evolution in seawater media. *Nano Res.* **2024**, *17*, 2429–2437.

[31] Song, H. Q.; Wu, M.; Tang, Z. Y.; Tse, J. S.; Yang, B.; Lu, S. Y. Single atom ruthenium-doped CoP/CDs nanosheets via splicing of carbon-dots for robust hydrogen production. *Angew. Chem., Int. Ed.* **2021**, *60*, 7234–7244.

[32] Zhao, Y. F.; Zhou, H.; Chen, W. X.; Tong, Y. J.; Zhao, C.; Lin, Y.; Jiang, Z.; Zhang, Q. W.; Xue, Z. G.; Cheong, W. C.et al. Two-step carbothermal welding to access atomically dispersed Pd_1 on three-dimensional zirconia nanonet for direct indole synthesis. *J. Am. Chem. Soc.* **2019**, *141*, 10590–10594.

[33] Tao, Y.; Guan, J. P.; Zhang, J.; Hu, S. Y.; Ma, R. Z.; Zheng, H. R.; Gong, J. X.; Zhuang, Z. C.; Liu, S. J.; Ou, H. H. et al. Ruthenium single atomic sites surrounding the support pit with exceptional photocatalytic activity. *Angew. Chem., Int. Ed.* **2024**, *63*, e202400625.

[34] Wang, Y.; Ma, F. Y.; Zhang, G. Q.; Zhang, J. W.; Zhao, H.; Dong, Y. M.; Wang, D. S. Precise synthesis of dual atom sites for electrocatalysis. *Nano Res.* **2024**, *17*, 9397–9427.

[35] Gao, Y.; Yang, C. D.; Sun, F. L.; He, D. P.; Wang, X. Q.; Chen, J.; Zheng, X. B.; Liu, R. C.; Pan, H. G.; Wang, D. S. Ligand-tuning metallic sites in molecular complexes for efficient water oxidation. *Angew. Chem., Int. Ed.* **2025**, *64*, e202415755.

[36] Zheng, X. B.; Yang, J. R.; Li, P.; Wang, Q. S.; Wu, J. B.; Zhang, E. H.; Chen, S. H.; Zhuang, Z. C.; Lai, W. H.; Dou, S. X. et al. Ir–Sn pair-site triggers key oxygen radical intermediate for efficient acidic water oxidation. *Sci. Adv.* **2023**, *9*, eadi8025.

[37] Chen, X. M.; Yuan, D.; Rong, C.; Wu, C.; Liu, P. R.; Liu, H. K.; Wang, D. S.; Dou, S. X.; Dou, Y. H. Single-atom catalysts supported on atomically thin materials for water splitting. *Adv. Powder Mater.* **2025**, *4*, 100330.

[38] Zheng, X. B.; Chen, Y. P.; Lai, W. H.; Li, P.; Ye, C. L.; Liu, N. N.; Dou, X. S.; Pan, H. G.; Sun, W. P. Electronegativity induced d-band center offset for Pt–Rh dual sites in high-entropy alloy boosts liquid fuels electrooxidation. *Adv. Funct. Mater.* **2022**, *32*, 2200663.

[39] Lv, Y. P.; Lin, L. L.; Xue, R. X.; Zhang, P. F.; Ma, F. Y.; Gan, T.; Zhang, J. W.; Gao, D. W.; Zheng, X. B.; Wang, L. G. et al. Electronegativity induced d-band center offset for Pt–Rh dual sites in high-entropy alloy boosts liquid fuels electrooxidation. *Adv. Energy Mater.* **2024**, *14*, 2304515.

[40] Yang, J. R.; Zhu, C. X.; Li, W. H.; Zheng, X. S.; Wang, D. S. Organocatalyst supported by a single-atom support accelerates both electrodes used in the chlor-alkali industry via modification of non-covalent interactions. *Angew. Chem., Int. Ed.* **2024**, *63*, e202314382.

[41] Xu, F. F.; Feng, B.; Shen, Z.; Chen, Y. Q.; Jiao, L.; Zhang, Y.; Tian, J. Y.; Zhang, J. R.; Wang, X. Z.; Yang, L. J. et al. Oxygen-bridged Cu binuclear sites for efficient electrocatalytic CO_2 reduction to ethanol at ultralow overpotential. *J. Am. Chem. Soc.* **2024**, *146*, 9365–9374.

[42] Zhao, J.; Zhang, Y. X.; Zhuang, Z. C.; Deng, Y. T.; Gao, G.; Li, J. Y.; Meng, A. L.; Li, G. C.; Wang, L.; Li, Z. J. et al. Tailoring d–p orbital hybridization to decipher the essential effects of heteroatom substitution on redox kinetics. *Angew. Chem., Int. Ed.* **2024**, *136*, e202404968.

[43] Gan, T.; Wang, D. S. Atomically dispersed materials: Ideal catalysts in atomic era. *Nano Res.* **2024**, *17*, 18–38.

[44] Guan, S. Y.; Yuan, Z. L.; Zhuang, Z. C.; Zhang, H. H.; Wen, H.; Fan, Y. P.; Li, B. J.; Wang, D. S.; Liu, B. Z. Why do single-atom alloys catalysts outperform both single-atom catalysts and nanocatalysts on MXene. *Angew. Chem., Int. Ed.* **2024**, *63*, e202316550.

[45] Tang, H. T.; Zhou, H. Y.; Pan, Y. M.; Zhang, J. L.; Cui, F. H.; Li, W. H.; Wang, D. S. Single-atom manganese-catalyzed oxygen evolution drives the electrochemical oxidation of silane to silanol. *Angew. Chem., Int. Ed.* **2024**, *63*, e202315032.

[46] Zhu, C. X.; Yang, J. R.; Zhang, J. W.; Wang, X. Q.; Gao, Y.; Wang, D. S.; Pan, H. G. Single-atom materials: The application in energy conversion. *Int. Mater.* **2024**, *3*, 74–86.

[47] Zhao, Y. F.; Jiang, W. J.; Zhang, J. Q.; Lovell, E. C.; Amal, R.; Han, Z. J.; Lu, X. Y. Anchoring sites engineering in single-atom catalysts for highly efficient electrochemical energy conversion reactions. *Adv. Mater.* **2021**, *33*, 2102801.

[48] Zhao, Y. F.; Lu, X. F.; Wu, Z. P.; Pei, Z. H.; Luan, D. Y.; Lou, X. W. Supporting trimetallic metal-organic frameworks on S/N-doped carbon macroporous fibers for highly efficient electrocatalytic oxygen evolution. *Adv. Mater.* **2023**, *35*, 2207888.

[49] Zhang, B.; Zheng, X. L.; Voznyy, O.; Comin, R.; Bajdich, M.; García-Melchor, M.; Han, L. L.; Xu, J. X.; Liu, M.; Zheng, L. R. et al. Homogeneously dispersed multimetal oxygen-evolving catalysts. *Science* **2016**, *352*, 333–337.

[50] Wang, L. P.; van Voorhis, T. Direct-coupling O_2 bond forming a pathway in cobalt oxide water oxidation catalysts. *J. Phys. Chem. Lett.* **2011**, *2*, 2200–2204.

[51] Chang, J. W.; Shi, Y. Y.; Wu, H.; Yu, J. K.; Jing, W.; Wang, S. Y.; Waterhouse, G. I. N.; Tang, Z. Y.; Lu, S. Y. Oxygen radical coupling on short-range ordered Ru atom arrays enables exceptional activity and stability for acidic water oxidation. *J. Am. Chem. Soc.* **2024**, *146*, 12958–12968.

[52] Lin, C.; Li, J. L.; Li, X. P.; Yang, S.; Luo, W.; Zhang, Y. J.; Kim, S. H.; Kim, D. H.; Shinde, S. S.; Li, Y. F. et al. *In-situ* reconstructed Ru atom array on α-MnO_2 with enhanced performance for acidic water oxidation. *Nat. Catal.* **2021**, *4*, 1012–1023.

[53] Rao, R. R.; Kolb, M. J.; Giordano, L.; Pedersen, A. F.; Katayama, Y.; Hwang, J.; Mehta, A.; You, H.; Lunger, J. R.; Zhou, H. et al. *Operando* identification of site-dependent water oxidation activity on ruthenium dioxide single-crystal surfaces. *Nat. Catal.* **2020**, *3*, 516–525.

[54] Liang, C. W.; Rao, R. R.; Svane, K. L.; Hadden, J. H. L.; Moss, B.; Scott, S. B.; Sachs, M.; Murawski, J.; Frandsen, A. M.; Riley, D. J. et al. Unravelling the effects of active site density and energetics on the water oxidation activity of iridium oxides. *Nat. Catal.* **2024**, *7*, 763–775.

[55] Sun, Y. M.; Liao, H. B.; Wang, J. R.; Chen, B.; Sun, S. N.; Ong, S. J. H.; Xi, S. B.; Diao, C. Z.; Du, Y. H.; Wang, J. O. et al. Covalency competition dominates the water oxidation structure–activity relationship on spinel oxides. *Nat. Catal.* **2020**, *3*, 554–563.

[56] Yu, Z. Y.; Duan, Y.; Kong, Y.; Zhang, X. L.; Feng, X. Y.; Chen, Y.; Wang, H. J.; Yu, X. X.; Ma, T.; Zheng, X. S. et al. General synthesis of tube-like nanostructured perovskite oxides with tunable transition metal-oxygen covalency for efficient water electrooxidation in neutral media. *J. Am. Chem. Soc.* **2022**, *144*, 13163–13173.

[57] Wu, H.; Chang, J. W.; Yu, J. K.; Wang, S. Y.; Hu, Z. A.; Waterhouse, G. I. N.; Yong, X.; Tang, Z. Y.; Chang, J. B.; Lu, S. Y. Atomically engineered interfaces inducing bridging oxygen-mediated deprotonation for enhanced oxygen evolution in acidic conditions. *Nat. Commun.* **2024**, *15*, 10315.

[58] Wang, L. Q.; Hung, S. F.; Zhao, S.; Wang, Y.; Bi, S. W.; Li, S. X.;

Ma, J. J.; Zhang, C. C.; Zhang, Y.; Li, L. L. et al. Modulating the covalency of Ru–O bonds by dynamic reconstruction for efficient acidic oxygen evolution. *Nat. Commun.* **2025**, *16*, 3502.

[59] Lee, S.; Lee, Y. J.; Lee, G.; Soon, A. Activated chemical bonds in nanoporous and amorphous iridium oxides favor low overpotential for oxygen evolution reaction. *Nat. Commun.* **2022**, *13*, 3171.

[60] Hao, S. Y.; Liu, M.; Pan, J. J.; Liu, X. N.; Tan, X. L.; Xu, N.; He, Y.; Lei, L. C.; Zhang, X. W. Dopants fixation of ruthenium for boosting acidic oxygen evolution stability and activity. *Nat. Commun.* **2020**, *11*, 5368.

[61] Ping, X. Y.; Liu, Y. D.; Zheng, L. X.; Song, Y.; Guo, L.; Chen, S. G.; Wei, Z. D. Locking the lattice oxygen in RuO_2 to stabilize highly active Ru sites in acidic water oxidation. *Nat. Commun.* **2024**, *15*, 2501.

[62] Li, A. L.; Kong, S.; Guo, C. X.; Ooka, H.; Adachi, K.; Hashizume, D.; Jiang, Q. K.; Han, H. X.; Xiao, J. P.; Nakamura, R. Enhancing the stability of cobalt spinel oxide towards sustainable oxygen evolution in acid. *Nat. Catal.* **2022**, *5*, 109–118.

[63] Gao, X. P.; Zhou, Y. N.; Tan, Y. J.; Liu, S. Q.; Cheng, Z. W.; Shen, Z. M. Graphyne doped with transition-metal single atoms as effective bifunctional electrocatalysts for water splitting. *Appl. Surf. Sci.* **2019**, *492*, 8–15.

[64] Li, A. L.; Kong, S.; Adachi, K.; Ooka, H.; Fushimi, K.; Jiang, Q. K.; Ofuchi, H.; Hamamoto, S.; Oura, M.; Higashi, K. et al. Atomically dispersed hexavalent iridium oxide from MnO_2 reduction for oxygen evolution catalysis. *Science* **2024**, *384*, 666–670.

[65] Ko, W.; Shim, J.; Ahn, H.; Kwon, H. J.; Lee, K.; Jung, Y.; Antink, W. H.; Lee, C. W.; Heo, S.; Lee, S. et al. Controlled structural activation of iridium single atom catalyst for high-performance proton exchange membrane water electrolysis. *J. Am. Chem. Soc.* **2025**, *147*, 2369–2379.

[66] Shi, Z. P.; Wang, Y.; Li, J.; Wang, X.; Wang, Y. B.; Li, Y.; Xu, W. L.; Jiang, Z.; Liu, C. P.; Xing, W. et al. Confined Ir single sites with triggered lattice oxygen redox: Toward boosted and sustained water oxidation catalysis. *Joule* **2021**, *5*, 2164–2176.

[67] Yao, Y. C.; Hu, S. L.; Chen, W. X.; Huang, Z. Q.; Wei, W. C.; Yao, T.; Liu, R. R.; Zang, K. T.; Wang, X. Q.; Wu, G. et al. Engineering the electronic structure of single atom Ru sites via compressive strain boosts acidic water oxidation electrocatalysis. *Nat. Catal.* **2019**, *2*, 304–313.

[68] Cao, L. L.; Luo, Q. Q.; Chen, J. J.; Wang, L.; Lin, Y.; Wang, H. J.; Liu, X. K.; Shen, X. Y.; Zhang, W.; Liu, W. et al. Dynamic oxygen adsorption on single-atomic ruthenium catalyst with high performance for acidic oxygen evolution reaction. *Nat. Commun.* **2019**, *10*, 4849.

[69] Li, J. J.; Fu, S. Q.; Wang, R. J.; Shi, W. J.; Zeng, Y. W.; Zhang, B. Surface sulfonic-group bonded oxygen evolution catalyst for proton exchange membrane water electrolysis. *Nat. Commun.* **2025**, *16*, 9910.

[70] Shan, J. Q.; Ye, C.; Chen, S. M.; Sun, T. L.; Jiao, Y.; Liu, L. M.; Zhu, C. Z.; Song, L.; Han, Y.; Jaroniec, M. et al. Short-range ordered iridium single atoms integrated into cobalt oxide spinel structure for highly efficient electrocatalytic water oxidation. *J. Am. Chem. Soc.* **2021**, *143, 13*, 5201–5211.

[71] Tang, J. Y.; Guan, D. Q.; Xu, H. Y.; Zhao, L. Q.; Arshad, U.; Fang, Z. J.; Zhu, T. J.; Kim, M.; Pao, C. W.; Hu, Z. W. et al. Undoped ruthenium oxide as a stable catalyst for the acidic oxygen evolution reaction. *Nat. Commun.* **2025**, *16*, 801.

[72] Qiao, X. S.; Kang, H. J.; Li, Y.; Cui, K.; Jia, X.; Wu, X. H.; Qin, W. Grain boundary density and electronic dual modulation of intermetallic Co_2B by Fe doping toward efficient catalyst for oxygen evolution reaction. *Appl. Catal. B: Environ.* **2022**, *305*, 121034.

[73] He, W. D.; Tan, X. H.; Guo, Y. Y.; Xiao, Y. H.; Cui, H.; Wang, C. X. Grain-boundary-rich RuO_2 porous nanosheet for efficient and stable acidic water oxidation. *Angew. Chem., Int. Ed.* **2024**, *63*, e202405798.

[74] Li, W. Q.; Hu, Z. Y.; Zhang, Z. W.; Wei, P.; Zhang, J. N.; Pu, Z. H.; Zhu, J. W.; He, D. P.; Mu, S. C.; van Tendeloo, G. Nano-single crystal coalesced PtCu nanospheres as robust bifunctional catalyst for hydrogen evolution and oxygen reduction reactions. *J. Catal.* **2019**, *375*, 164–170.

[75] Zhang, J. Y.; Qian, J. M.; Ran, J. Q.; Xi, P. X.; Yang, L. J.; Gao, D. Q. Engineering lower coordination atoms onto NiO/Co_3O_4 heterointerfaces for boosting oxygen evolution reactions. *ACS Catal.* **2020**, *10*, 12376–12384.

[76] Zhu, Y. P.; Guo, C. X.; Zheng, Y.; Qiao, S. Z. Surface and interface engineering of noble-metal-free electrocatalysts for efficient energy conversion processes. *Acc. Chem. Res.* **2017**, *50*, 915–923.

[77] Hao, Y. X.; Hung, S. F.; Wang, L. Q.; Deng, L. M.; Zeng, W. J.; Zhang, C. C.; Lin, Z. Y.; Kuo, C. H.; Wang, Y.; Zhang, Y. et al. Designing neighboring-site activation of single atom via tunnel ions for boosting acidic oxygen evolution. *Nat. Commun.* **2024**, *15*, 8015.

[78] Chen, J. H.; Ma, Y. R.; Cheng, C.; Huang, T.; Luo, R. H.; Xu, J. W.; Wang, X. Y.; Jiang, T. L.; Liu, H. X.; Liu, S. et al. Cobalt-doped $Ru@RuO_2$ core–shell heterostructure for efficient acidic water oxidation in low-Ru-loading proton exchange membrane water electrolyzers. *J. Am. Chem. Soc.* **2025**, *147*, 8720–8731.

[79] Liu, Y.; Huang, Y.; Wu, D. J.; Jang, H.; Wu, J. H.; Li, H. R.; Li, W. X.; Zhu, F.; Kim, M. G.; Zhou, D. L. et al. Ultrathin and conformal depletion layer of core/shell heterojunction enables efficient and stable acidic water oxidation. *J. Am. Chem. Soc.* **2024**, *146*, 26897–26908.

[80] Lu, Q.; Liu, J. J.; Zou, X, H.; Huang, B. R.; Wu, W. X.; Yin, J.; Liu, Z. Q.; Wang, Y. Breaking the activity-stability trade-off of RuO_2 via metallic Ru bilateral regulation for acidic oxygen evolution reaction. *Angew. Chem., Int. Ed.* **2025**, *64*, e202503733.

[81] Chen, J. Y.; Cui, P. X.; Zhao, G. Q.; Rui, K.; Lao, M. M.; Chen, Y. P.; Zheng, X. S.; Jiang, Y. Z.; Pan, H. G.; Dou, S. X. et al. Low-coordinate iridium oxide confined on graphitic carbon nitride for highly efficient oxygen evolution. *Angew. Chem., Int. Ed.* **2019**, *58*, 12540–12544.

[82] Abdullah, M. I.; Shao, J.; Fang, Y. S.; Wu, X. B.; Hu, M. Q.; Tao, Y. K.; Wang. H. J. Tackling activity-stability paradox of reconstructed $NiIrO_x$ electrocatalysts by bridged W–O moiety. *Nat. Commun.* **2024**, *15*, 10587.

[83] Ram, R.; Xia, L.; Benzidi, H.; Guha, A.; Golovanova, V.; Manjón, A. G.; Rauret, D. L.; Berman, P. S.; Dimitropoulos, M.; Mundet, B. et al. Water-hydroxide trapping in cobalt tungstate for proton exchange membrane water electrolysis. *Science* **2024**, *384*, 1373–1380.

[84] Shi, Z. P.; Li, J.; Wang, Y. B.; Liu, S. W.; Zhu, J. B.; Yang, J. H.; Wang, X.; Ni, J.; Jiang, Z.; Zhang, L. J. et al. Customized reaction route for ruthenium oxide towards stabilized water oxidation in high-performance PEM electrolyzers. *Nat. Commun.* **2023**, *14*, 843.

[85] Wang, Y.; Yang, R.; Ding, Y. J.; Zhang, B.; Li, H.; Bai, B.; Li, M. R.; Cui, Y.; Xiao, J. P.; Wu, Z. S. Unraveling oxygen vacancy site mechanism of Rh-doped RuO_2 catalyst for long-lasting acidic water oxidation. *Nat. Commun.* **2023**, *14*, 1412.

[86] Zhu, W. J.; Yao, F.; Cheng, K. J.; Zhao, M. T.; Yang, C. J.; Dong, C. L.; Hong, Q. M.; Jiang, Q.; Wang, Z. C.; Liang, H. F. Direct dioxygen radical coupling driven by octahedral ruthenium-oxygen-cobalt collaborative coordination for acidic oxygen evolution reaction. *J. Am. Chem. Soc.* **2023**, *145*, 17995–18006.

[87] Zhang, J. H.; Fu, X. B.; Kwon, S.; Chen, K. F.; Liu, X. Z.; Yang, J.; Sun, H. R.; Wang, Y. C.; Uchiyama, T.; Uchimoto, Y. et al. Tantalum-stabilized ruthenium oxide electrocatalysts for industrial water electrolysis. *Science* **2025**, *387*, 48–55.

[88] Dang, Q.; Lin, H. P.; Fan, Z. L.; Ma, L.; Shao, Q.; Ji, Y. J.; Zheng, F. F.; Geng, S. Z.; Yang, S. Z.; Kong, N. N. et al. Iridium metallene oxide for acidic oxygen evolution catalysis. *Nat. Commun.* **2021**, *12*, 6007.

[89] Fan, Z. L.; Ji, Y. J.; Shao, Q.; Geng, S. Z.; Zhu, W. X.; Liu, Y.; Liao,

F.; Hu, Z. W.; Chang, Y. C.; Pao, C. W. et al. Extraordinary acidic oxygen evolution on new phase 3R-iridium oxide. *Joule* **2021**, *5*, 3221–3234.

[90] Yu, G.; Li, R. L.; Hu, Y. M.; Lin, X. E.; Lin, Z.; Wu, D. Y.; Wang, G. M.; Hong, X. Supporting IrO_x nanosheets on hollow TiO_2 for highly efficient acidic water splitting. *Nano Res.* **2024**, *17*, 6903–6909.

[91] Madika, B.; Saha, A.; Kang, C.; Buyantogtokh, B.; Agar, J.; Wolverton, C. M.; Voorhees, P.; Littlewood, P.; Kalinin, S.; Hong, S. Artificial intelligence for materials discovery, development, and optimization. *ACS Nano* **2025**, *19*, 27116–27158.

[92] Yang, X. Y.; Zhou, K.; He, X.; Zhang, L. J. Methods and applications of machine learning in computational design of optoelectronic semiconductors. *Sci. China Mater.* **2024**, *67*, 1042–1081.

[93] Butler, K. T.; Davies, D. W.; Cartwright, H.; Isayev, O.; Walsh, A. Machine learning for molecular and materials science. *Nature* **2018**, *559*, 547–555.

[94] Lin, X. Y.; Du, X. W.; Wu, S. C.; Zhen, S. Y.; Liu, W.; Pei, C. L.; Zhang, P.; Zhao, Z. J.; Gong, J. L. Machine learning-assisted dual-atom sites design with interpretable descriptors unifying electrocatalytic reactions. *Nat. Commun.* **2024**, *15*, 8169.

[95] Jia, X.; Zhou, Z. H.; Liu, F. Z.; Wang, T. Y.; Wang, Y. H.; Zhang, D.; Liu, H.; Wang, Y.; Ye, S. B.; Amezawa, K. et al. Closed-loop framework for discovering stable and low-cost bifunctional metal oxide catalysts for efficient electrocatalytic water splitting in acid. *J. Am. Chem. Soc.* **2025**, *147*, 22642–22654.

[96] Li, X. Y.; Liu, Z. H.; Gao, A.; Zhang, Q. H.; Zhong, H.; Meng, F. Q.; Lin, T.; Wang, S. Y.; Su, D.; Jin, K. J. et al. Ferroelastically protected reversible orthorhombic to monoclinic-like phase transition in ZrO_2 nanocrystals. *Nat. Mater.* **2024**, *23*, 1077–1084.

[97] Espinosa, M. R.; Guerrero, F.; Kazmierczak, N. P.; Oyala, P. H.; Hong, A.; Hadt, R. G.; Agapie, T. Slow electron spin relaxation at ambient temperatures with copper coordinated by a rigid macrocyclic ligand. *J. Am. Chem. Soc.* **2025**, *147*, 14036–14042.

[98] Luo, Y. H.; Du, X. H.; Wu, L. L.; Wang, Y. J.; Li, J. D.; Ricardez-Sandoval, L. Machine-learning-accelerated screening of double-atom/cluster electrocatalysts for the oxygen reduction reaction. *J. Phys. Chem. C* **2023**, *127*, 20372–20384.

[99] Quan, L.; Zhao, X.; Yang, L. M.; You, B.; Xia, B. Y. Intrinsic activity identification of noble metal single-sites for electrocatalytic chlorine evolution. *Angew. Chem., Int. Ed.* **2025**, *64*, e202414202.